Similarity analysis of the momentum field of a subsonic, plane air jet with varying jet-exit and local Reynolds numbers

Ravinesh C. Deo, Graham J. Nathan, and Jianchun Mi

Citation: Phys. Fluids **25**, 015115 (2013); doi: 10.1063/1.4776782
View online: http://dx.doi.org/10.1063/1.4776782
View Table of Contents: http://pof.aip.org/resource/1/PHFLE6/v25/i1
Published by the American Institute of Physics.

PHYSICS OF FLUIDS **25**, 015115 (2013)

Similarity analysis of the momentum field of a subsonic, plane air jet with varying jet-exit and local Reynolds numbers

Ravinesh C. Deo,[1,a)] Graham J. Nathan,[2] and Jianchun Mi[3]
[1]*University of Southern Queensland, Faculty of Sciences, Department of Mathematics and Computing, Springfield, QLD 4300, Australia*
[2]*The University of Adelaide, School of Mechanical Engineering, Adelaide, Australia*
[3]*College of Engineering, Peking University, China*

(Received 14 August 2012; accepted 2 January 2013; published online 25 January 2013)

A similarity analysis is presented of the momentum field of a subsonic, plane air jet over the range of the jet-exit Reynolds number Re_h ($\equiv U_b h/\upsilon$ where U_b is the area-averaged exit velocity, h the slot height, and υ the kinematic viscosity) = 1500 − 16 500. In accordance with similarity principles, the mass flow rates, shear-layer momentum thicknesses, and integral length scales corresponding to the size of large-scale coherent eddy structures are found to increase linearly with the downstream distance from the nozzle exit (x) for all Re_h. The autocorrelation measurements performed in the near jet confirmed reduced scale of the larger coherent eddies for increased Re_h. The mean local Reynolds number, measured on the centerline and turbulent local Reynolds number measured in the shear-layer increases non-linearly following $x^{1/2}$, and so does the Taylor microscale local Reynolds number that scales as $x^{1/4}$. Consequently, the comparatively larger local Reynolds number for jets produced at higher Re_h causes self-preservation of the fluctuating velocity closer to the nozzle exit plane. The near-field region characterized by over-shoots in turbulent kinetic energy spectra confirms the presence of large-scale eddy structures in the energy production zone. However, the faster rate of increase of the local Reynolds number with increasing x for jets measured at larger Re_h is found to be associated with a wider inertial sub-range of the compensated energy spectra, where the −5/3 power law is noted. The downstream region corresponding to the production zone persists for longer x/h for jets measured at lower Re_h. As Re_h is increased, the larger width of the sub-range confirms the narrower dissipative range within the energy spectra. The variations of the dissipation rate (ε) of turbulent kinetic energy and the Kolmogorov (η) and Taylor (λ) microscales all obey similarity relationships, $\varepsilon h/U_b^3 \sim Re_h^3$, $\eta/h \sim {Re_h}^{-3/4}$, and $\lambda/h \sim {Re_h}^{-1/2}$. Finally, the underlying physical mechanisms related to discernible self-similar states and flow structures due to disparities in Re_h and local Reynolds number is discussed. [http://dx.doi.org/10.1063/1.4776782]

I. INTRODUCTION

Research interest into turbulent plane jets has been elevating since the pioneering works of Schlichting,[1] Forthman,[2] and Bickley.[3] This is because the flow statistics of these jets, described by the mean, turbulent, and higher order velocity and scalar moments are represented as two-dimensional fields. This statistical two-dimensionality is valuable for understanding the control and transport of mixing processes[4] so these jets remain prototypical flows of relevance to engineering applications

a)Author to whom correspondence should be addressed. Electronic addresses: ravinesh.deo@usq.edu.au and physrcd@yahoo.com. Telephone: +61 (07) 3470 4430.

in propulsion, combustion, ventilation, air conditioning, and other environmental systems. The simplified flow statistics offer advantages in basic turbulence research and mathematical applications such as numerical modeling, validation of models, and investigating the large and small-scale eddy structures in moving fluids.[5,6] Nevertheless, there are far fewer investigations of plane jets than of their round-jet counterparts. Henceforth, this article is devoted to furthering the understanding of the role of large and small-scale structures in turbulent plane jets.

A plane jet is generated by a rectangular slot, whose dimension ($w \times h$) is characterized by the aspect ratio, $AR = w/h$, with $w \gg h$, where w and h are measured along the spanwise (z) and lateral (y) directions, respectively (Fig. 1). Two parallel sidewalls attached to either end of the primary jet restrict fluid entrainment along the spanwise (z) direction, so that the velocity component, $W(x, y)$ along the z-plane is nominally taken to be zero. The self-sustaining jet is approximated to originate from a concentrated (line) source of momentum and is typically analysed for the case where it issues into a quiescent (stagnant) or a co-flowing environment. The main freestream velocity, $U(x, y)$ decays in the streamwise (x) direction that is also accompanied by jet spreading in the y-direction which is proportional to the entrainment velocity, $V(x, y)$.

For a smoothly contoured nozzle, the time-averaged mean flow exhibits a potential core region immediately downstream of the exit up to an axial distance of $4 < x/h < 6$, in which $U(x, y)$ is uniform so that the mean centerline velocity, $U_c(x, 0)$ approximately equals the bulk mean velocity, U_b (Fig. 1). Within the interaction zone ($6 < x/h < 20$), the large-scale eddy structures interact with the ambient flow to transport gross momentum flux along the x-direction.[7,8] In the self-similar field, the jet becomes self-preserving where statistical properties such as jet spreading and velocity decay rates, turbulence intensity, etc. become invariant. Despite the voluminous research quantifying basic statistical parameters of plane jet flows, several aspects of the similarity behavior, especially with respect to the flow structure, remain unevaluated.

One fundamental parameter known to influence the downstream development, evolution, and self-preservation of a jet is the jet-exit Reynolds number (Re_h) which for a plane jet, is usually defined by

$$\mathrm{Re}_h = U_b h/\upsilon. \tag{1}$$

Here U_b is the area-averaged bulk mean velocity, υ is the kinematic viscosity of fluid, and h is the characteristic length scale of the nozzle, which is mostly taken as the smallest dimension of the nozzle, i.e., the "height" when the jet issues horizontally. The investigations of Lemieux and Oosthuizen[9] for Re_h between $700 \leq Re_h \leq 4200$, Suresh *et al.*[10] between $250 \leq Re_h \leq 6250$ and Klein *et al.*[11] for $Re_h \leq 6000$ identified that Re_h exerts a substantial influence on most of the basic flow statistics. However, these studies were limited to the relatively low Re_h range that only extended into the lower end of the turbulent regime. The investigation by Namar and Otugen[12] extended this range slightly to consider $1000 \leq Re_h \leq 7000$, but their nozzle was not constrained by sidewalls, and hence does not conform to the requirement for a fully planar jet.[13] While the measurements by Everitt and Robbins[14] covered Re_h between $16\,000 \leq Re_h \leq 75\,000$, their study does not isolate the influence of Re_h from other initial conditions since they simultaneously varied the AR between 21 and 128. That is, their work does not separate the effect of Re_h from that of AR, which is also known to influence the flow statistics.[15,16]

To our best knowledge, the first independent study of the dependence of flow statistics of plane jets from the low to moderate ranges of Re_h between $1500 \leq Re_h \leq 57\,500$ was reported by Deo *et al.*[17] That study demonstrated that the self-preserving magnitudes of jet decaying and spreading rates decreased with Re_h, while the turbulence intensity, the skewness, and flatness factors increased asymptotically with it. The study also identified an initial increase in the dimensionless frequency of primary vortices with Re_h, but this increase did not extend to higher values of Re_h. Also, the flow structure of jets driven by dynamical changes in the large and small-scale vortices in the near and self-similar fields has not been explored previously.

Another parameter of relevance that typically characterizes a jet's shear layer development is the momentum thickness, θ_m. This quantity is believed to scale with the size of large-scale eddy

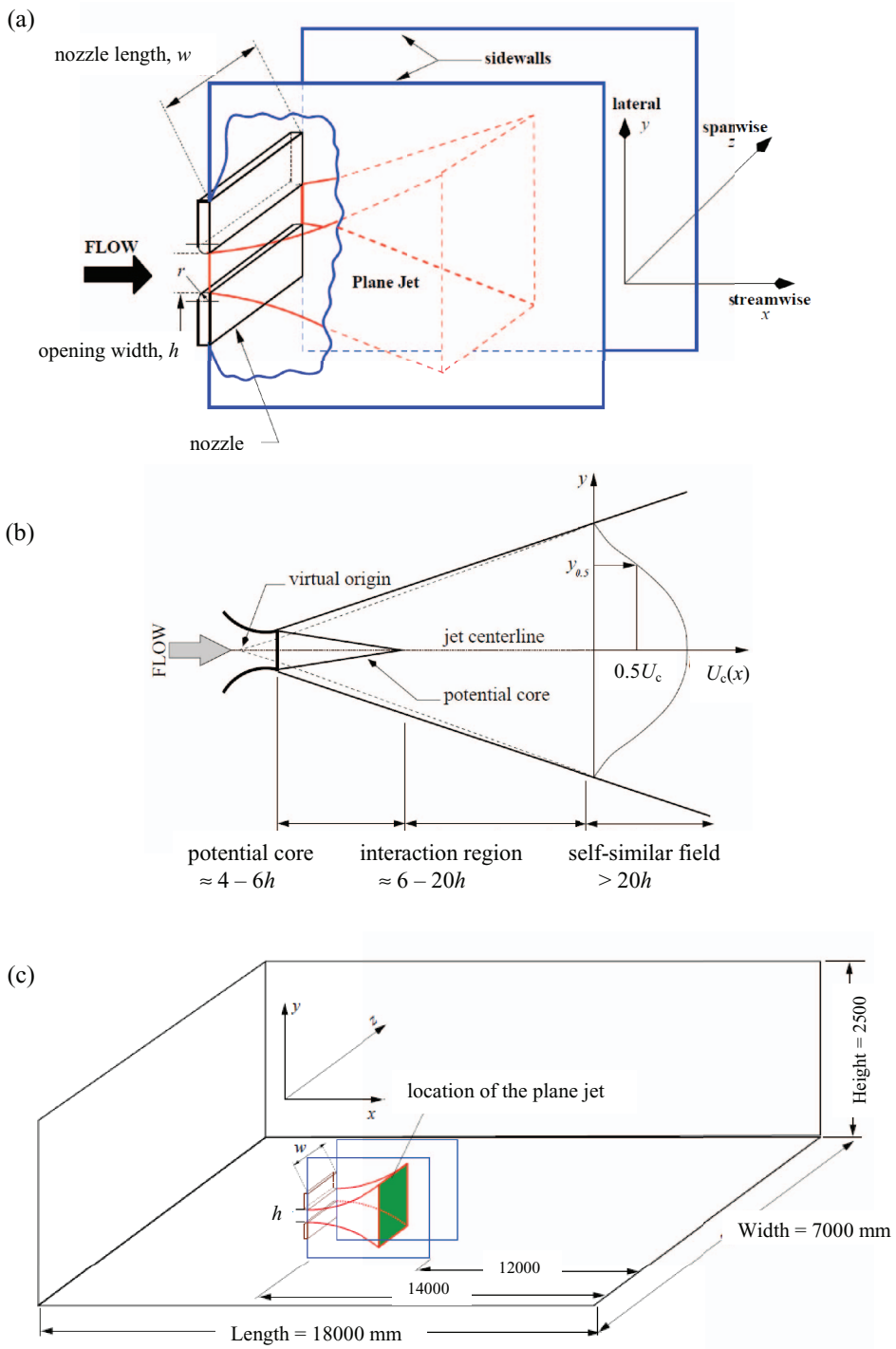

FIG. 1. (a) A schematic of the plane jet nozzle, (b) time-averaged flow, and (c) laboratory dimensions. Note: $U_c \equiv$ centerline mean velocity, $y_{0.5} \equiv$ half-width (y-value where $U(x, y) = 1/2U_c(x)$).

structures generated by the shear-layer roll-up process.[18] Such an effect is known to prevail in the case of round and non-circular jets[19,20] although there is substantial paucity of experimental data of this phenomenon for the case of a plane jet. At the exit plane, θ_m characterizes the initial shear layer, which in turn influences the growth and development of the large-scale eddies including the double roller-like vortices shed in the von-Karman sheets.[21] Further downstream, θ_m characterizes the jet

spread, and is numerically obtained for any value of x by integrating the mean velocity, $U(x, y)$

$$\theta_m(x) = \int_{y=0}^{y=\infty} \left(\frac{U(x, y)}{U_c(x)}\right)\left(1 - \frac{U(x, y)}{U_c(x)}\right) dy. \tag{2}$$

Several studies have demonstrated that the axial growth of $\theta_m(x)$, and of the large-scale eddies on which this growth depends, is a function of Re_h.[4,11,12] However, the role of the *local* Reynolds number, Re_θ, based on the scale, $\theta_{\rm m}(x)$, is less clear in previous literature although this parameter is also known to evolve non-identically for jets measured at different Re_h.[17] This is because, unlike a round jet where the Re_θ is invariant, or for a planar wake flow where Re_θ decreases,[22] that in a plane jet Re_θ increases with x.[17] This suggests that the relative importance of viscosity on self-preservation appears to diminish with increasing x. However, the axial location of the self-preserved state due to increasing Re_θ is not well understood, and its dependence on initial and boundary conditions especially on a plane jet remains to be explored.

Johansson *et al.*[22] showed that the turbulent kinetic energy spectra of a planar wake flow exhibits unique regions of the inertial sub-range that satisfy the Kolmogorov's −5/3 power law for different Reynolds numbers but this phenomenon remains unexplored for a plane jet. Based on a similar view, George[23] postulated that similarity solutions for a planar wake flow measured at high Reynolds number will apply if there is a conspicuous inertial sub-range in the spectra to ensure the scales of motion are effectively inviscid. However, the separate influences of Re_h and Re_θ on the self-preservation through their effects on the flow structure, especially for a plane jet, have received less attention.

Similarly, to our best knowledge, less is known on the influences of Re_h and Re_θ on θ_m (x) and on the energy spectra of a plane jet. The present investigation aims to bridge this gap by revisiting the underlying theory behind self-preservation by analysis of experimental data of a series of sub-sonic plane air jets measured for Reynolds numbers, $1500 \leq Re_h \leq 16\,500$. The physical mechanisms driving discernible flow structures for jets with varying Re_h are explored using spectral, autocorrelation, and probability density analysis of the instantaneous velocity signal in the near and the far fields.

II. ANALYTICAL OVERVIEW

The time-averaged mean momentum equation for a two-dimensional, incompressible plane jet (neglecting spanwise motion along the z axis) is given by the modified Navier-Stokes and the continuity equations, respectively,

$$U\frac{\partial U}{\partial x} + V\frac{\partial U}{\partial y} = -\frac{\partial}{\partial y}\langle uv\rangle \quad \text{and} \quad \frac{\partial U}{\partial x} + \frac{\partial V}{\partial y} = 0, \tag{3}$$

where U, u, and V, v are the components of the mean and turbulent velocity along the x and y-direction, respectively, and $\langle uv\rangle$ is the Reynolds shear stresses term. For the case of a plane jet, the x-direction is the general direction of mean propagation and y-direction is the direction of mean jet spread. In the self-preserving field, the distributions of the streamwise component of mean velocity $U(x, y)$ and root-mean-square velocity $\langle u(x, y)^2\rangle^{1/2}$, and transverse component of mean velocity $V(x, y)$, and root-mean-square velocity $\langle v(x, y)^2\rangle^{1/2}$ are represented by

$$U(x, y) = U_c(x)\ F'(\eta), \qquad V(x, y) = U_c(x)F'(\eta) \tag{4}$$

and

$$< u(x, y) >^2 = U_c^2(x)g(\eta), < v(x, y) >^2 = U_c^2(x)g(\eta), < u(x, y)\ v(x, y) > = U_c^2(x)g^2(\eta). \tag{5}$$

Likewise, the normalisation of $U(x, y)$ and $V(x, y)$ by $U_c(x)$ yields the Reichardt's similarity solution (e.g., Ref. 24),

$$\frac{U(x,y)}{U_c(x,0)} = \exp(-\ln 0.5\ \eta^2),\ \frac{V(x,y)}{U_c(x,0)} = \frac{C}{4}\left[4\eta\exp(-\eta^2\ln 2) - \sqrt{\pi}erf(-\eta\sqrt{2\ln 2})\right], \tag{6}$$

where $\eta = y(x)/y_{0.5}(x)$, $y_{0.5}(x)$ is the y-location where $U(x, y) = 1/2U_c(x)$, the error function $erf(\eta) = \frac{2}{\sqrt{\pi}}\int_0^\eta e^{-\xi^2}d\xi$ and $F(\eta)$ and $g(\eta)$ are smooth functions $= 0$ at $y = 0$. The momentum equation (3) and expressions for U and V are used to solve for the Reynolds stress as

$$\frac{< u(x,y)\ v(x,y) >}{U^2{}_c(x)} = \frac{\sqrt{\pi}C}{4}\exp(-\eta^2)\ erf(\eta). \tag{7}$$

Differentiating (4) with respect to x, substituting for η and clearing the redundant terms yields

$$\frac{\partial U}{\partial x} = U_c^{'}(x)\,F'(\eta) - U_c(x)\frac{y_{0.5}^{'}(x)\ \eta}{y_{0.5}(x)}F''(\eta), \qquad \frac{\partial U}{\partial y} = \frac{U_c(x)}{y_{0.5}(x)}F''(\eta). \tag{8}$$

Applying the freestream and continuity conditions (3) and substituting into (7) results in

$$\begin{aligned} V &= \int_0^y \frac{\partial V}{\partial y}dy \quad = -\int_0^y \frac{\partial U}{\partial x}dy \\ &= U_c(x)\ y_{0.5}^{'}(x)\,\eta F'(\eta) - [U_c(x)\,y_{0.5}(x)]'\ \ [F(\eta) - F(0)]. \end{aligned} \tag{9}$$

The partial derivative of the Reynolds stress equation (5) with respect to y yields

$$\frac{\partial}{\partial y}\langle u\ v\rangle = \frac{U_c^2(x)}{y_{0.5}(x)}g'(\eta). \tag{10}$$

Substituting (10) into (3) and rearranging the terms yields

$$\frac{U_c^{'}(x)\ y_{0.5}(x)}{U_c(x)}\ F'^2 - \frac{[U_c\ y_{0.5}(x)]'}{U_c(x)}FF'' + g = 0. \tag{11}$$

For the case of a self-preserving jet, the coefficients in Eq. (11) must be constant since $U_c(x)$ and $y_{0.5}(x)$ are functions of x only.[25] It thus follows that $y_{0.5}\ (x) \sim x$ since $dy_{0.5}/dx$ is constant in the self-preserving field.

The similarity of the large-scale, mean jet flow obeys solutions of the form, $\theta_m\ (x) \sim x$ and $U_c\ (x) \sim x^{-1/2}$ and $y_{0.5}\ (x) \sim x$ as previously so that

$$\frac{U_c(x)}{U_b} = \left[K_u\left(\frac{x - x_{01}}{h}\right)\right]^{-1/2} = K_u^{-1/2}\xi^{-1/2}, \tag{12}$$

$$\frac{y_{0.5}(x)}{h} = K_y\left(\frac{x - x_{02}}{h}\right) = K_y\,\xi, \tag{13}$$

$$\frac{\theta(x)}{h} = K_\theta\left(\frac{x - x_{03}}{h}\right) = K_\theta\,\xi, \tag{14}$$

where K_u, K_y, K_θ are the velocity decay, jet spreading, and shear layer growth rates, and x_{01}, x_{02}, and x_{03} are the virtual origins in Eqs. (12)–(14).

From the practical point of view, one of the most valuable properties of the mean jet flow is the entrainment (E) measured by the mass flow rate, $m(x)$, at any x relative to the initial value m_o at $x = 0$. Since the jet is to spread laterally, E is proportional to the ratio of $m(x)$ to m_o so that

$$E \equiv \frac{m(x)}{m_o} = \frac{1}{hU_b} \int_{-\infty}^{+\infty} U(x, y)dy \tag{15}$$

to obey a similarity solution of the form $m(x)/m_0 \sim U_c(x)/U_b$, where the $U_c(x) \sim x^{-1/2}$ substituted into Eq. (15) yields

$$\left(\frac{m(x)}{m_o}\right)^2 = K_m \left(\frac{x - x_{04}}{h}\right) = K_m \, \xi, \tag{16}$$

where K_m is associated with the entrainment induced by large and small-scales, and is subject to initial conditions of the jet flow.

In accordance with theoretical arguments of George,[23] we define the centerline value of the mean *local* Reynolds number Re_θ of a plane jet, based on two length scales, $\theta_m(x)$ and $y_{0.5}(x)$ as

$$\mathrm{Re}_\theta(x) = \frac{U_c(x)\,\theta_m(x)}{\nu} \text{ and } \mathrm{Re}_{y_{0.5}}(x) = \frac{U_c(x) y_{0.5}(x)}{\nu}. \tag{17}$$

Following Eqs. (12)–(14) that $U_c \sim x^{-1/2}$, $\theta_m(x) \sim x$, and $y_{0.5} \sim x$, the Re_θ varies as $x^{-1/2} \times x^1 \sim x^{1/2}$. Based on this, similarity analysis indicates that irrespective of the initial value of Re_h, all plane jets will eventually attain high local Reynolds numbers if measured at sufficiently great downstream distances. Accordingly, this downstream location should correlate with their unique transition to non-identical self-similar states, depending on the value of Re_h.

To seek similarity solutions for the Re-dependence of the small-scale flow, consider a plane jet where the turbulent kinetic energy produced by mean motion of the large-scale eddies at low wave numbers that are localized over a region, $\Lambda(x)$. At sufficiently high Reynolds number, it is usually considered that the centerline dissipation rate $\varepsilon_c(x)$ of the turbulent kinetic energy (E_k) by the smallest eddies equals the supply from the large-scale eddies, e.g., Ref. 26. Thus

$$\varepsilon_c(x) \equiv \frac{U_c^3(x)}{y_{0.5}(x)} \text{ and } \varepsilon_c(x) = 15\upsilon \left\langle \left(\frac{\partial u_c(x)}{\partial x}\right)^2 \right\rangle, \tag{18}$$

where the small-scale eddies convect downstream with a velocity that scales cubically with $U_c(x)$, and that $E_k(x) \equiv 1/2 < u^2 + v^2 + w^2 > \approx 3/2 < u^2 >$ in locally isotropic turbulence. In accordance with Kolmogorov's theory[27]

$$\eta = \left(\frac{\nu^3}{\varepsilon}\right)^{1/4}, \tag{19}$$

which gives

$$\eta/\Lambda \sim \mathrm{Re}_h^{-3/4}, \tag{20}$$

if one incorporates $<u^2>^{1/2} \equiv (2E_k/3)^{1/2}$ into $\mathrm{Re}_h = E_k^2/\varepsilon\nu$ by stating that $\Lambda \equiv (E_k)^{3/2}/\varepsilon$, where Λ and η are large-scale (production range) and small-scale (dissipative range) eddies in the self-preserving jet.

Several previous studies, e.g., Refs. 26–29 have consistently verified the inertial sub-range in spectra of E_k for a self-similar jets where the turbulent eddy motions of length scale equals the Taylor's transverse microscale (λ). Incorporating $\varepsilon(x)$ into $u^2/\lambda^2 = (\overline{\partial u}/\partial x)^2$ and $E_k = \frac{3}{2} < u^2 >^{1/2}$ yields

$$\lambda = \sqrt{\frac{15\nu u^2}{\varepsilon}} = \sqrt{\frac{10\nu E_k}{\varepsilon}}, \tag{21}$$

where the inequality $\Lambda < \lambda < \eta$ is *a priori* following Eqs. (18)–(21). That is, the self-preservation of isotropic turbulence requires the scale of the inertial sub-range eddies to measure in between the

scale of the largest (production-scale) and the smallest (dissipation-scale) eddies. Some manipulation of Eq. (21) yields

$$\lambda/\Lambda \equiv \sqrt{10}\,\mathrm{Re}_h^{-1/2} \tag{22}$$

and

$$\lambda/\eta \equiv \sqrt{10}\,\mathrm{Re}_h^{1/4}. \tag{23}$$

We now seek similarity solutions for the x-dependence of small-scale flow statistics. In accordance with Eq. (18), $\varepsilon_c(x)$ varies as ${U^3}_c(x)/y_{0.5}(x)$. Substituting $U_c \sim x^{-1/2}$ and $y_{0.5} \sim x$ yields

$$\varepsilon(x) \sim x^{-5/2}. \tag{24}$$

Likewise, based on Eqs. (19)–(21), self-similarity requires that $\eta(x) \sim \varepsilon(x)^{-1/4}$ and $\lambda(x) \sim \varepsilon(x)^{-1/2}$ whose incorporation into Eq. (24) yields the x-dependence of Kolmogorov and Taylor microscales

$$\eta(x) \sim x^{5/8} \tag{25}$$

and

$$\lambda(x) \sim x^{3/4}. \tag{26}$$

Combining the x and Re_h dependence of both microscales yields similarity relationships for small-scale statistics in the self-preserving plane jet

$$\frac{\varepsilon h}{U_b^3} = K_\varepsilon\,(x/h)^{-5/2}\,, \tag{27}$$

$$\frac{\eta}{h} = K_{1,\varepsilon}^{-1/4}\,\mathrm{Re}_h^{-3/4}\,(x/h)^{5/8}\,, \tag{28}$$

$$\frac{\lambda}{h} = K_{2,\varepsilon}^{-1/2}\,\mathrm{Re}_h^{-1/2}\,(x/h)^{3/4}\,, \tag{29}$$

where the experimental constants K_ε, $K_{1\varepsilon}$, and $K_{2\varepsilon}$ are subject to initial conditions.

III. EXPERIMENTAL DESIGN

A. Plane jet facility

The present experiment is described in detail elsewhere (e.g., Refs. 17 and 30) so is only summarized in this article. All data were collected in the Fluid Mechanics Laboratory (Fig. 1(c)) located within the School of Mechanical Engineering at The University of Adelaide, Australia. Air was supplied by an open circuit wind tunnel driven by a variable-speed, 14.5 kW aerofoil-type centrifugal motor. The mainstream flow was pre-conditioned by a wide angle diffuser, settling chamber, honeycomb, and screens to feed a large polynomial contraction of the tunnel. The exit of the contraction measured 720 mm × 340 mm where the plane jet nozzle was clamped. The nozzle was constructed from two perspex plates separated by slot height $h = 5.6$ mm and width $w = 340$ mm. The upstream edges were radially contoured with $r = 12$ mm. Consequently, the design ensured a sufficiently large aspect ratio $AR = w/h = 60$ necessary to produce a statistically two-dimensional jet far into the self-preserving region[13] together with the nozzle profile-contraction factor $r^* = r/h \approx 2.14$ necessary to generate a mean velocity profile resembling the Blasius curve.[31]

B. Hot wire anemometry

A constant temperature anemometer employing single hot wire probes operating at an overheat ratio of 1.5 was chosen. Custom-designed sensors were constructed to minimize heat losses along the

lengths of the wire and for the resolution of small-scale structures in jets measured at different Re_h. The length (l_w) and diameter (d_w) of the sensor was chosen based on previous research following Browne *et al.*[8] who used $l_w/d_w \approx 208$ and Champagne[32] who used $l_w/d_w \approx 160$ to resolve fine-scale turbulence structures in their jets. Bradshaw[33] stated that the heat loss from a sensor is ≈15% when $l_w/d_w \approx 200$. Bearing in mind that l_w and d_w are critical parameters, we chose copper-plated tungsten sensors of $l_w \approx 1$ mm and $d_w = 5$ μm to yield $l_w/d_w \approx 200$. A three-dimensional traverse enabled measuring instruments to be traversed laterally (across the jet) and axially (direction of the mean flow). The mean static pressure was monitored with a Pitot static tube for the calibration of the hot wire sensor. The streamwise component of the instantaneous velocity, $U(x)$ was measured on the centerline between the locations $0 \leq x/h \leq 160$, while the lateral velocity component $U(x, y)$ was measured at selected x/h (across all jets) for different Re_h.

For the present measurements, a PC-30F data acquisition system was utilized. The system has a 200 kHz multi-channel analogue to digital (A/D) converter with a 12-bit (≈ 2.4 mV) resolution. After monitoring the real-time raw velocity signal on a Tektronix Oscilloscope, all data were visualized in WaveView 2.0 (DOS based data interface) for preliminary inspection. The input range of A/D board chosen was ± 5.0 V so an appropriate offset was applied to the sampled voltage to rectify the signal into the ± 3.0 V range. This avoided clipping some important tails of the higher order moments of the fluctuating signal.[34] A cut-off frequency, $f_c = 9.2$ kHz was used to sample data at a Nyquist frequency of 18.4 kHz for 22.4 s to collect approximately 4×10^5 data samples per measurement location.

It is acknowledged that stationary hot-wire measurements may downgrade the accuracy of the present measurements especially near the outer edge of the jet where turbulence intensity is relatively high. In this region greater amplitudes of the fluctuating velocities can produce erroneous values of the small-scale statistics especially those calculated using the Taylor's hypothesis. In such cases, flying-hot wire or Laser Doppler Velocimetry (LDV) techniques should be employed for better resolution of the flow properties.[35] However, in this article we are interested in comparing the relative magnitudes of the flow statistics for different Re_h so it is hoped that such errors are absorbed proportionally into the individual jet measurements. Some portion of such redundant noise is also removed by the digital filtering scheme adopted from Mi *et al.*[40] prior to resolving the small-scale statistics. This helps determine as correctly as possible the dissipation rates even though the data acquisition rate is fixed for every downstream location and different cases of Re_h.

Based on the present hot-wire calibrations and the observed scatter in the analysed data, the uncertainties in the mean quantities within the jet's shear layer are estimated to be ∼4.0% and those on the jet's centre-plane are ∼0.8%. The estimated errors in the turbulent quantities amount to ∼2.0% and the integral quantities (momentum thickness and mass flow rates) are ∼3.0%. The estimated errors in the small-scale statistics are as follows: (ε ±4.0%; η ± 1.0%; λ ± 6.0%).

C. Jet exit conditions

The volumetric flow rates through the jet facility spanned the range $7.6 \times 10^{-3} \leq Q \leq 8.4 \times 10^{-2}$ m^{3}s^{-1} which corresponded to Reynolds numbers, $1500 \leq Re_h \leq 16\,500$ and Mach numbers, $M = U_b/c$ of $0.01 \leq M \leq 0.13$ (where c is the speed of sound in ambience). The Mach numbers confirmed that these isothermal jets were subsonic, quasi-steady, and incompressible. As such, the simplified incompressible models used for the analysis of self-preservation are appropriate. The measurement of the lateral distributions of mean and fluctuating velocity close to the exit plane ($x/h \approx 0.5$) showed subtle dependence on Re_h.[17] Although all cases produced an approximately "top-hat" velocity profile, small differences were found for the different cases under investigation. As Re_h was increased, the velocity profiles became flatter, with a larger region of flow uniformity.

The jet-exit conditions are determined by the normalized values of δ_m and θ_m (at $x/h = 0.5$) previously reported for same plane jet by Deo *et al.*[17] (Fig. 2(a)). The same parameters for a high-AR rectangular jet by Namar and Otugen[12] are also included. For the present plane jets, the increase in Re_h produced an asymptotic decrease in θ_m and δ_m, which is in agreement with the trends noted for round jets[36] and high-AR rectangular jets.[12] However, the shape factor H increased asymptotically with Re_h to approach a constant value of 2.6, that accorded with that of a laminar Blasius profile for

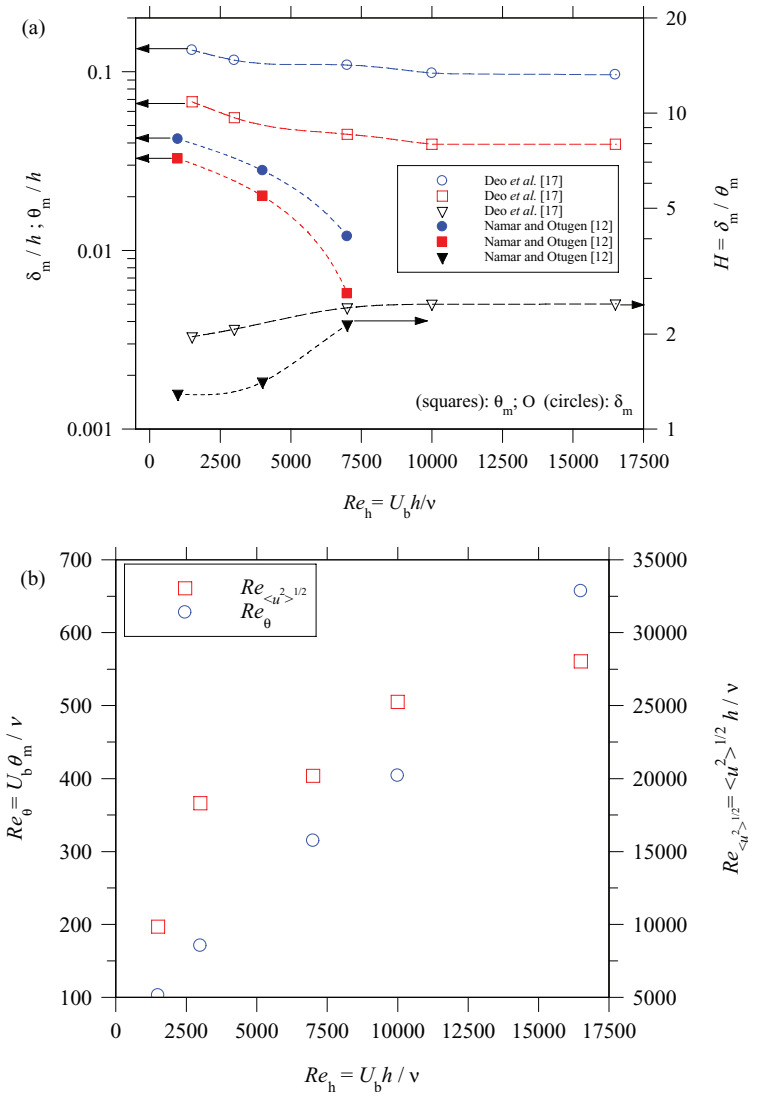

FIG. 2. The jet-exit conditions defined by (a) displacement thickness (δ_m), momentum thickness (θ_m) and shape factors (H) at $x/h = 0.5$ reported by Deo *et al.*[17] (b) Momentum-based Reynolds number (Re_θ) and shear layer-peak turbulent Reynolds number ($\mathrm{Re}_{<u_p>^{1/2}}$) measured at $x/h = 0.25$. In part (a), δ_m and θ_m at $x/h = 1$ for high-AR rectangular jet of Namar and Otugen[12] are shown.

the cases $Re_h \geq 10\,000$. The decrease in displacement and momentum thickness for increased Re_h is expected because we have changed Re_h by varying the jet exit velocity.

That H increases with increasing Re_h to approach the Blasius value for $Re_h > 10\,000$ demonstrates that the radial contraction of the nozzle is effective in producing a nearly laminar flow at the exit plane. Note that a direct comparison of the magnitudes of present δ_m and θ_m with Namar's values is unreasonable because the latter jet was measured at a different downstream location and was configured without sidewalls along the x-y plane. Despite the present decrease in θ_m with Re_h, the momentum-based Reynolds number (Re_θ) increased linearly (Fig. 2(b)). However, the normalized values of the shear layer turbulence intensity ($< u^2_p >^{1/2} / U_c$) decreased with increasing Re_h, although the opposite trend is found for the peak rms-based Reynolds number, $\mathrm{Re}_{<u_p>^{1/2}} = < u_p^2 >^{1/2} h/\upsilon$. That is, the exit shear layer of the jet with the highest Re_h depicted high initial unsteadiness despite the laminar mean velocity profile. Hence too, the instabilities of the initial shear layer of this jet are expected to decrease with increased Re_h.

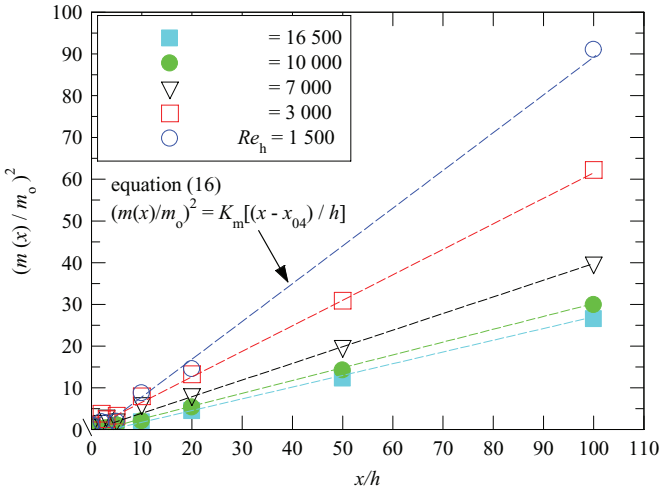

FIG. 3. Streamwise evolution of mass flow rates $m(x)$ normalized by bulk mass flow rate (m_0) at the exit plane.

IV. RESULTS AND GENERAL DISCUSSION

A. Mean and turbulent statistics

Figure 3 presents the streamwise variations of the kinematic mass flow rates $(m(x)/m_o)^2$ as a function of x/h for all cases investigated. Notice that the mass flow rates have been derived indirectly from the lateral (y-direction) profiles of mean velocity, $U(x, y)$ reported previously by Deo *et al.*[17] In accordance with the similarity Eq. (16), all experimental data obey the relationship $m(x) \sim x^{1/2}$ for $x/h \geq 10$ when the mean flow has become self-preserving. It is also clear that the self-preserving low Re_h jet exhibits a higher mass flow rate than its high Re_h counterparts, which is self-evident from the direct measurements showing identical trends in the velocity decay and jet spreading rates.[10,12,17,30] Additionally, the gross entrainment rates (K_m) and the x-location of virtual origins of mass flow (x_{03}) for each measured jet is Re-dependent (Fig. 4). As with the previously reported trends of K_y and x_{02},[17] K_m and x_{03} decrease asymptotically with increasing Re_h so that the horizontal asymptote of the former attains a value of ≈0.26 for the two high-Re cases.

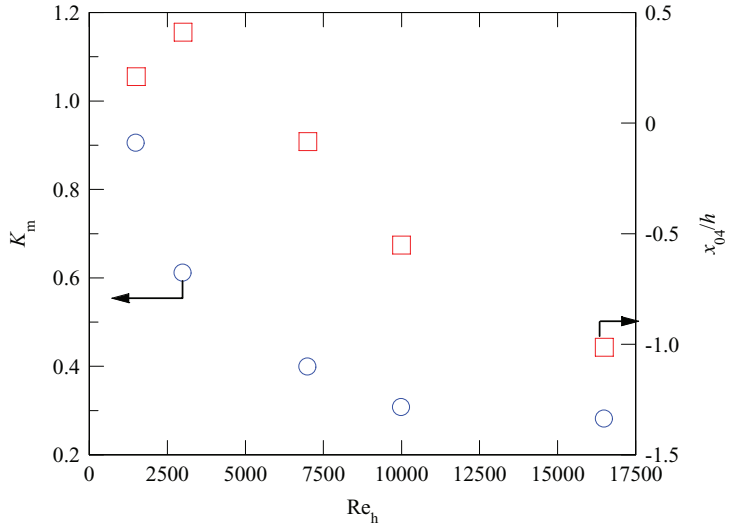

FIG. 4. Dependence of entrainment rates (K_m) and virtual origin (x_{04}/h) on Re_h.

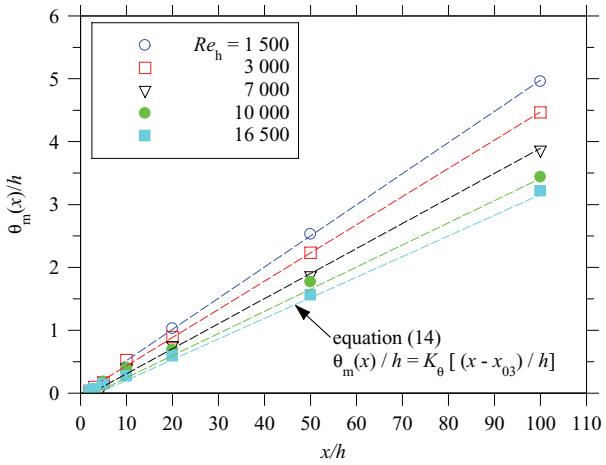

FIG. 5. Streamwise evolutions of momentum thickness $\theta_m(x)$ for various Re_h.

The increased entrainment rates of low Re_h jets over the high Re_h cases are correlated with increased momentum thicknesses $\theta_m(x)$ of their shear layers (Fig. 5), which also follows the previously reported trends of linear growth of the jet half-widths, e.g., Ref. 17. The linear rise in $\theta_m(x)$ with increasing x is consistent with the previously reported trends of increased jet half-width[17] and is in accordance with the similarity analysis of a plane jet (Sec. II). A smaller value of $\theta_m(x)$ indicates lesser deficit in the shear-layer momentum, which is consistent with similarity equation (2). Imperatively, the high-Re jets appear to be nominally more inviscid than their low-Re_h counterparts at any downstream location which explains their low momentum thicknesses. Since the shear layer growth rates are proportional to $\theta_m(x)$, which in turn characterizes the scale of larger structures, it is deduced that the size of these eddies decrease with increasing Re_h. Similar were the observations of Bogey and Bailly[18] for round jet measurements.

Figure 6 displays the dependence on Re_h on K_θ and l_m where K_θ represents the growth rate of the shear-layer in the linear regime and l_m is the mixing length based on Prandtl's hypothesis. Evidently, K_θ decreases asymptotically with increasing Re_h which is consistent with the previously reported data of Deo *et al.*[17] The mixing length (l_m) in a self-preserving plane jet is proportional to its spreading rate K_y to exhibit the relationship $l_m \approx 0.09 K_y$.[37,38] This empiricism emerges from the uniform eddy

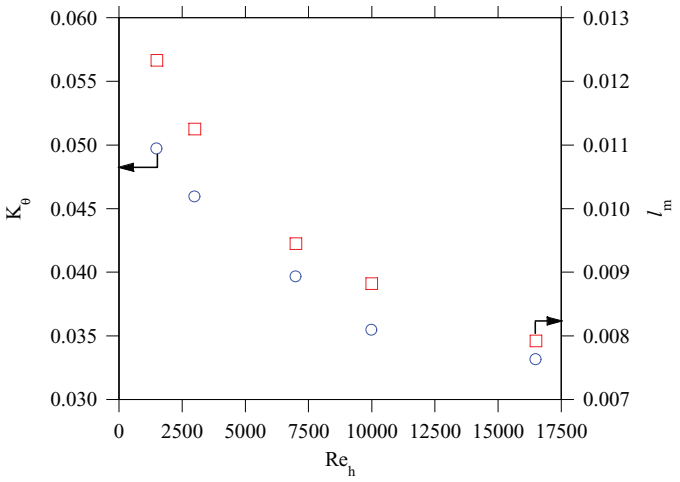

FIG. 6. The Re_h-dependence of the shear-layer growth rate (K_θ) and mixing length (l_m) based on Prandtl's mixing length hypothesis where l_m is proportional to K_y as embodied in Eq. (13).

viscosity model that advocates the proportionality equation $\nu_T = l_m^2 \left| \frac{\partial U}{\partial y} \right| = \frac{l_m^2(x) U_c(x)}{y_{0.5}(x)} \left| F''(\eta) \right|$.[39] However, the similarity analyses depicting that υ_T varies as $x^{1/2}$ appears to be a limitation of the eddy viscosity model as it suggests that the plane jet is not a perfect self-similar flow.

Figure 6 (right ordinate) demonstrates that l_m like K_θ, also decreases asymptotically with increasing Re_h indicating that the spatial domain of the mixing regime shrinks when Reynolds number is increased.

The characteristic size of the large-scale eddy structures (Λ) is estimated for each Re_h using the auto-correlation functions, R_{uu} (Δx, 0, 0) of the fluctuating velocity (u). Here R_{uu} (Δx, 0, 0) convolutes the instantaneous velocity, u, at a given point, x_0, and given time lag, $\tau = 0$ to another time, $\tau + \Delta\tau$, and displacement $x_0 + \Delta x$. According to Taylor's transformation, τ is linked to the eddy separation distance ($r = x_0 + \Delta x$) where $r(\Delta x) = U_c(x)\tau(\Delta t)$. Based on this, the size of large-scale eddies (Λ) is estimated viz $\Lambda = \int_{(x=0, R_{uu}=1)}^{(x=\Delta x, R_{u,u}=0)} R_{uu}(\Delta x, 0, 0)\, d\Delta x$ from $\Delta x = 0$ to a separation distance, r.[40] As per Figure 7, $\Lambda(x)$ increases linearly with x for all cases of investigation to accord with the similarity relationship

$$\frac{\Lambda(x)}{h} = K_\Lambda \left(\frac{x - x_{05}}{h} \right) = K_\Lambda\, \xi. \tag{30}$$

In the similarity equation (30), K_Λ represents the growth rate of the large-scale eddies, and x_{05} is some virtual origin. Based on the present data, the size of eddies, denoted by the magnitude of $\Lambda(x)$, decreases for increased Re_h. Furthermore, the value of K_Λ is found to decrease asymptotically with increasing Re_h, which is also in agreement with the deductions of Figure 6 and the previous round jet data of Bogey and Bailly.[18] It is noteworthy that the trend coincides with a slight increase in the Strouhal number of eddies in the potential core region, as reported previously by Deo *et al.*[17] and elsewhere by Suresh *et al.*[10]

Figures 8(a) and 8(b) display the evolution of the two different forms of the mean local Reynolds number $\mathrm{Re}_\theta(x) = U_c(x)\theta_m(x)/\upsilon$ and $\mathrm{Re}_{y_{0.5}}(x) = U_c(x)y_{0.5}(x)/\upsilon$, where $\theta_m(x)$ and $y_{0.5}(x)$ are the characteristic length scales of jets with different values of Re_h. The similarity relationships embodied in Eq. (17) ($Re_\theta(x) \sim x^{1/2}$ and $Re_{y0.5}(x) \sim x^{1/2}$) are well demonstrated for all cases of Re_h. This relationship is verified unambiguously, in Figure 8(b) where plot of $Re_{y0.5}(x)$ versus $x_{\mathrm{norm}} = \sqrt{x}$ shows reasonably good linear trends with generally good collapse of data within the experimental

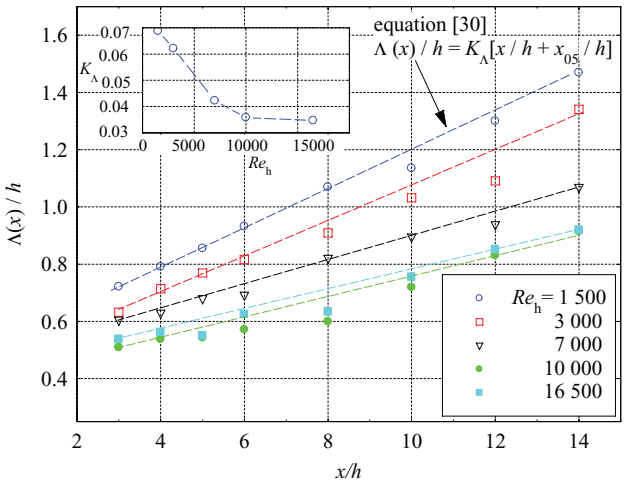

FIG. 7. Streamwise evolutions of the integral length scale, $\Lambda\ (x)\ /h$ for various cases of Re_h. The asymptotic decrease of K_Λ with increasing Re_h is shown in the inset.

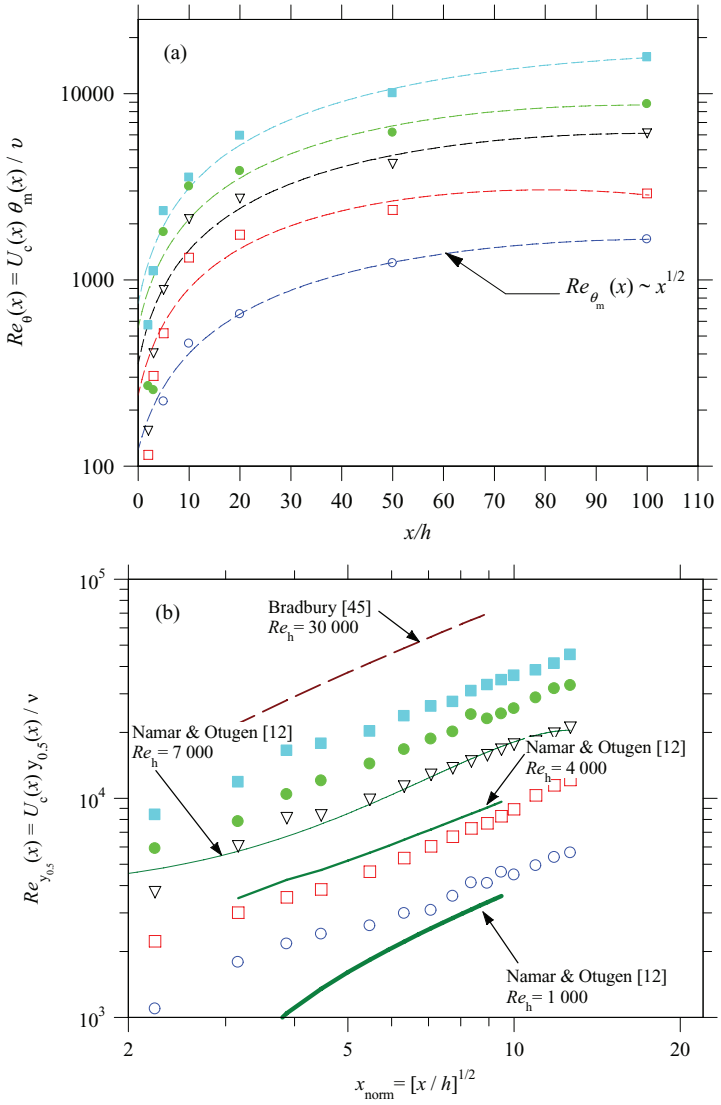

FIG. 8. Streamwise evolutions of (a) local Reynolds number (Re_θ) based on mean momentum thickness $\theta_m(x)$, (b) local Reynolds number ($Re_{y0.5}$) based on jet half-widths $y_{0.5}(x)$. Note that part (b) has been modified after Deo[30] and Deo *et al.*[17]

errors. This sort of dependence exists in previous data showing that plane jets exhibit higher K_y than their corresponding K_u values irrespective of the magnitude of Re_h [Fig. 6; Fig. 9(b) of Ref. 17].

Accordingly, it is deduced that $U_c(x) \sim 1/\sqrt{K_u}$ and $y_{0.5}(x) \sim K_y$, so a slower decay rate of $U_c(x)$ relative to $y_{0.5}(x)$ and $\theta_m(x)$ is self-evident. Despite the square root growth of $Re_\theta(x)$ with x, every case tested characterises unique values of $Re_\theta(x)$ at any given downstream location. However, the actual magnitude of the mean local Reynolds number is correspondingly higher for a jet measured at a larger Re_h. Our results agree qualitatively with those of Namar and Otugen[12] for high-AR rectangular jets (reproduced in Fig. 9(b)) and other investigations on plane jet flows.[4,45]

The one-dimensional streamwise component of the turbulent kinetic energy $E_k(x)$ is displayed in Figure 9 where $E_k(x)$ normalized by $U^2{}_c(x)$. The data of Namar and Otugen[12] for the cases Re_h = 1000–7000 are also included. As with the previously reported data on the rms of fluctuating velocity, $E_k(x)/U_c^2(x)$ exhibits a rapid rate of initial increase with x to acquire a local maximum for all Re_h. Interestingly, the maximum values are strongly dependent on Re_h. These differences are consistent with the unique scaling of the large eddy structures with increasing downstream distance (Fig. 6). In accordance with Dracos *et al.*,[52] the large-scale eddy structures are primarily

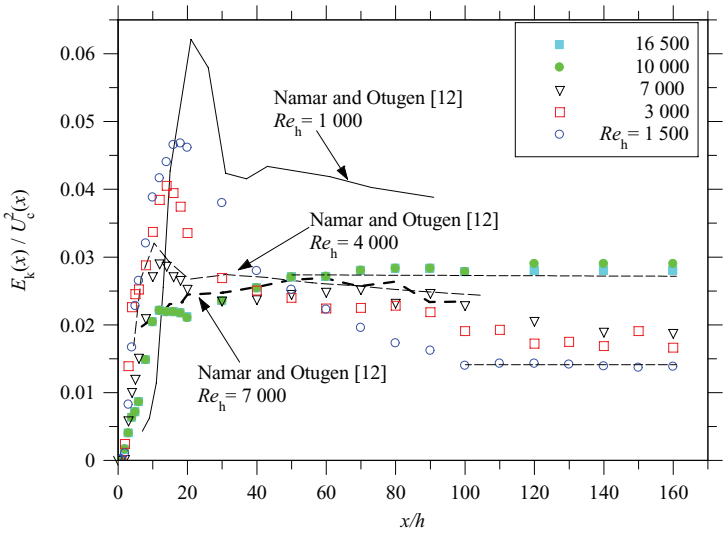

FIG. 9. Streamwise evolution of the one-dimensional turbulent kinetic energy E_k normalized by $U^2{}_c(x)$ together with the data of Namar and Otugen.[12]

responsible for most anisotropic behavior in the propagated jets. It is deduced that low-Re_h cases exhibit higher anisotropic behavior than high-Re_h counterparts, and hence possess more ordered large-scale structures that are evidenced by consistently larger values of $E_k(x)/U_c^2(x)$ and more rapid growth rate of momentum thicknesses within the shear layers (see Figs. 5 and 6).

A closer examination of Figure 9 shows the upstream shift in the peak turbulent kinetic energy with increasing Re_h. The comparatively larger peak supports decreased momentum thickness and reduced size of large-scale eddy structures in high-Re jets (Figs. 5 and 18) that accords with the direct numerical simulations of round jet flows by Bogey and Bailly.[18] The low-Re jet produces substantially higher turbulent kinetic energy than its high-Re counterparts at identical x-locations. For example, at $x/h = 20$, $E_k(x)/U^2{}_c(x) = 4.62 \times 10^{-2}$ for $Re_h = 1500$, which is double the corresponding value of 2.09×10^{-2} for $Re_h = 16\,500$. Again, this difference is associated with stronger anisotropic turbulence in the near field of the low-Re jet as also confirmed later (see Fig. 25(b)) where a slower rate of decay of the autocorrelation coefficient (R_{uu}) is depicted.

Consistent with well-known views on self-preservation (e.g., Ref. 47), no net turbulent kinetic energy is produced in the far field, as $E_k(x)/U^2{}_c(x)$ becomes invariant for all cases of investigation (Fig. 9). However, the magnitude of $E_k(x)/U^2{}_c(x)$ and x-locations where this invariance occurs along the x-plane strongly depends on Re_h, and the corresponding local Reynolds number acquired by these jets.

It is noteworthy that, in accordance with local Reynolds number effects, the asymptotic invariance of $E_k(x)/U^2{}_c(x)$ is realized at a shorter axial distance ($x/h \approx 40$) for $Re_h = 16\,500$ compared to $x/h = 100$ for $Re_h = 1500$. This correlates with a mean local Reynolds number, $Re_{y0.5}\,(x) \approx 40\,000$ for the former jet relative to $Re_{y0.5}\,(x) \approx 5000$ for the latter. Clearly the acquisition of substantially large mean local Reynolds number for the high-Re jet appears to determine the x-location of the onset of self-preservation, as also confirmed later, by spectral analysis (Sec. IV C). Furthermore, the magnitude of self-preserving values of the turbulent kinetic energy is discernible for each tested case; with low Re-jets sustaining a greater amount of energy than their high-Re counterparts.

Figure 10 checks the self-preserving behavior within the lateral distributions of turbulence intensity $u_n = \langle u(x, y)^{1/2}/U_c(x)\rangle$ measured across the present jets. Except the case $Re_h = 1500$, all turbulence intensity profiles exhibit self-similar behavior at some value of x/h, although the x-locations are dependent on Re_h. That is, for cases of $Re_h = 3000$, 7000 and $\geq 10\,000$, u_n becomes congruent for approximately $x/h \geq 50$, 20, and 10, respectively. Clearly, the different x-location at which self-preservation of the turbulence intensity profiles is achieved depends on Re_h.

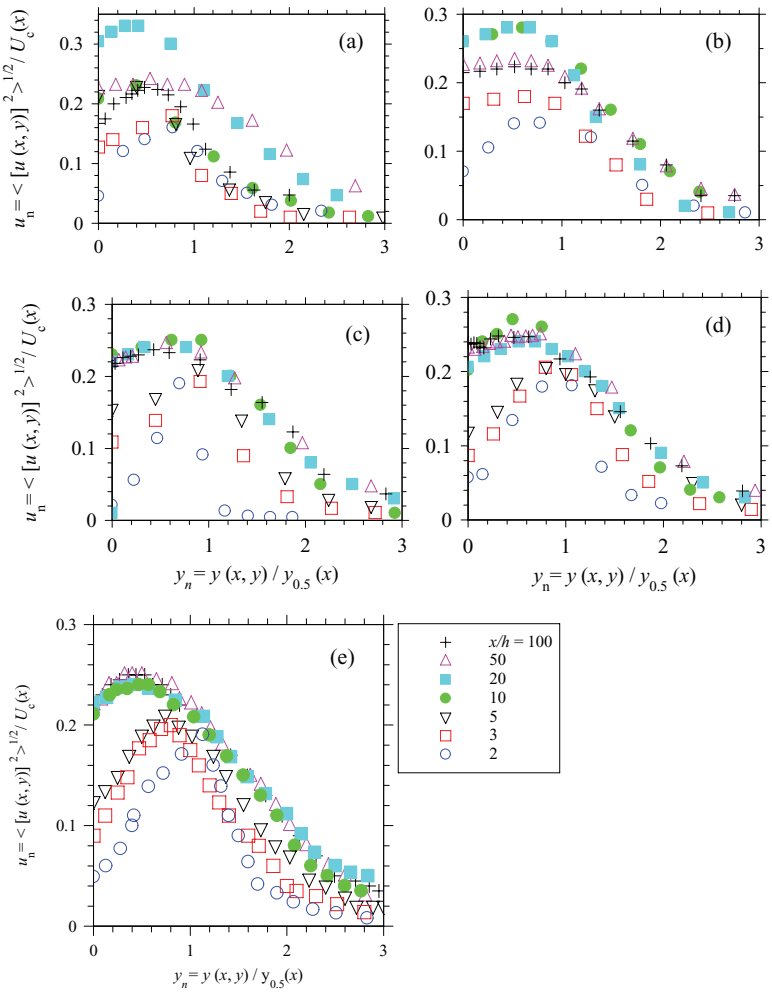

FIG. 10. Lateral profiles of turbulence intensity $u_n = <[u(x, y)]>^{1/2}/U_c(x)$ measured across the jet for Re_h = (a) 1500, (b) 3000, (c) 7000, (d) 10 000, and (e) 16 500.

Figure 11 examines the asymptotic invariance of $\langle u_c^2(x)\rangle^{1/2}/U_c(x)$ with respect to Re_θ (x) for the cases $Re_h \geq 3000$. It is demonstrated that the self-preservation of plane jets is attained at approximately identical values of $Re_\theta \sim 2500$, irrespective of Re_h, despite some scatter, particularly for lower Re_h. Again, this confirms the key role of high local Reynolds number for attaining self-preservation of turbulent properties of the present plane jets.

Figure 11 displays the streamwise evolutions of the turbulent local Reynolds number, $\mathrm{Re}_{\langle u_p^2\rangle^{1/2},y0.5}(x) = \langle u_p^2(x)\rangle^{1/2} y_{0.5}(x)/\nu$ in the jet's shear-layer. Here, the characteristic scales used are $y_{0.5}(x)$ = jet half width and $\langle u_p^2(x)\rangle^{1/2} \equiv$ peak shear-layer turbulence intensity at its corresponding downstream locations. Similar to the trends for the mean local Reynolds number (Fig. 8), the turbulent local Reynolds number increases with $x^{1/2}$ although the absolute values of $\mathrm{Re}_{y0.5}(x)$ and $\mathrm{Re}_{\langle u_p^2\rangle^{1/2},y0.5}(x)$ are somewhat different due to different lengths scaled used (i.e., $U_c(x)$ versus $\langle u_p^2(x)\rangle^{1/2}$). However, the square-root scaling ensures that, no matter how low the initial Re_h is, all plane jets will eventually attain sufficiently large turbulent Reynolds number in the self-preserving field if measured at great downstream distance from the exit plane.

Comparing Figure 12 with Figure 10, the lateral profiles of the turbulence intensity became congruent at $x/h \approx 10$ for $Re_h \geq 16\,500$. This corresponded to a turbulent local Reynolds number of $\mathrm{Re}_{\langle u_p^2\rangle^{1/2},y0.5}(x) = 2\,650$ (Fig. 12). However, the congruency emerged at $x/h \approx 50$ for Re_h

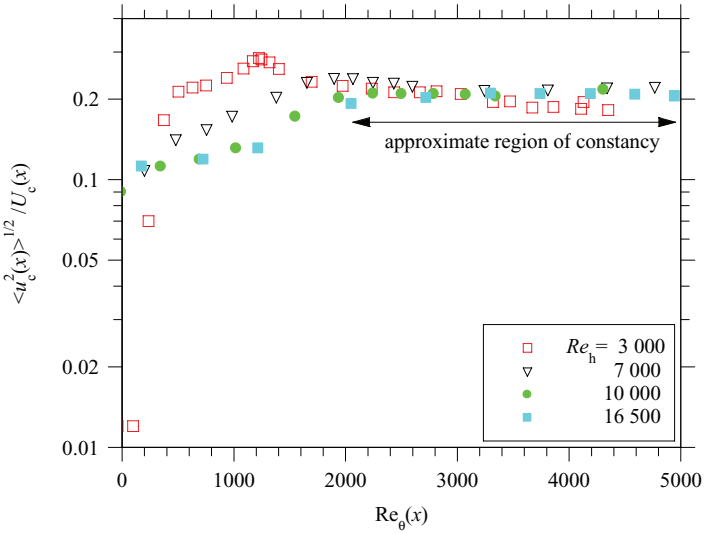

FIG. 11. Dependence of streamwise turbulence intensity $\langle u_c^2(x)\rangle^{1/2}/U_c(x)$ on $Re_\theta(x)$ for $Re_h = 3000$–16 500.

$= 3000$, where the corresponding turbulent local Reynolds number was $\mathrm{Re}_{\langle u_p^2\rangle^{1/2},y_{0.5}}(x) = 1000$. This provides overwhelming support that a relatively large value of turbulent local Reynolds number is necessary for the self-preserving state to evolve. This requirement reinforces the view that the role of viscosity diminishes when the mean and turbulent local Reynolds numbers are large enough to allow the onset of the self-preserving state.

Figure 13 plots the streamwise evolution of the peak turbulence intensity, $\langle u_c^2(x)\rangle^{1/2}/U_c(x)$ within a transverse profile at that axial distance. It is noted that both properties increase monotonically from nearly zero to reach an absolute maximum value over the range $5 < x/h < 20$ for $Re_h \geq 7000$. This location, however, appears to be dependent on Re_h. The substantially larger peaks for high-Re jets are associated with the production of more coherent, large-scale eddy structures. As deduced previously (Fig. 7), these eddies are generally smaller than those compared with low-Re jets. Further,

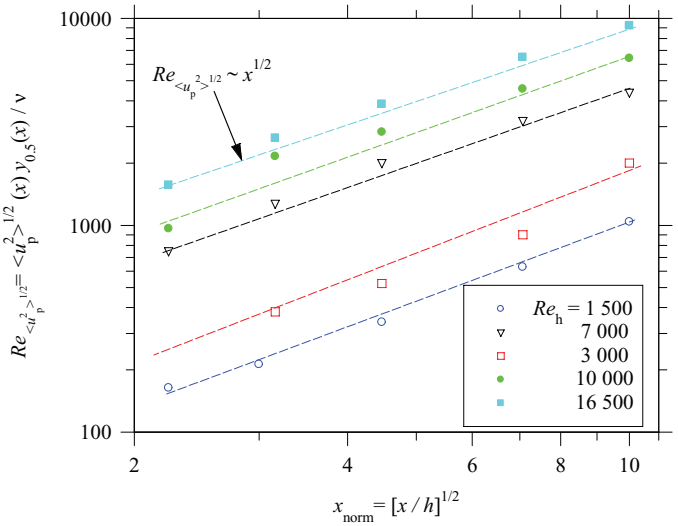

FIG. 12. Streamwise evolutions of the local turbulent Reynolds number $\mathrm{Re}_{<u_p^2>^{1/2},y_{0.5}}(x) = < u_p^2(x) >^{1/2} y_{0.5}(x)/\nu$. Note: $< u^2{}_{\mathrm{p}}(x) >^{1/2} \equiv$ peak value of shear layer turbulence intensity $y_{0.5}\,(x) \equiv$ jet half-width and $< u^2{}_{\mathrm{p}}(x) >^{1/2}$ is deduced from Fig. 10.

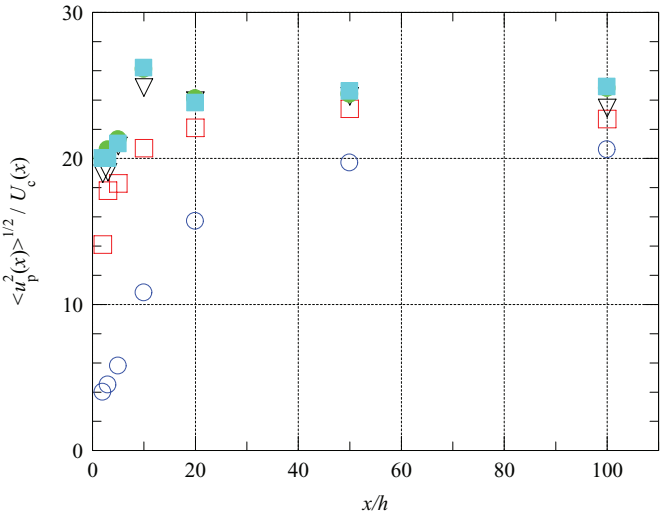

FIG. 13. Streamwise evolutions of the peak shear-layer turbulence intensity, $< u^2{}_{\rm p}(x) >^{1/2} / U_{\rm c}(x)$ in %. Symbols are identical to Fig. 12.

the lower the Re_h, the greater is the axial distance where the peak is realised, which accords with the trends noted for the centerline turbulent kinetic energy (Fig. 9) and higher momentum thicknesses (Fig. 5). For all measured jets, the magnitudes of $\left\langle u_c^2(x)\right\rangle^{1/2} / U_c(x)$ decay with increasing x/h as the jet becomes self-preserving despite discernible differences among the different cases of Re_h. For example, at $x/h = 100$, the $Re_h = 16\,500$ registers turbulence intensity values approximately fourteen times larger values than the case $Re_h = 1500$ (Fig. 13(a)). Additionally, it is found that the peak shear-layer turbulence intensity did not attain self-preservation within the measured range of x/h for this jet.

Figure 14 presents the transverse profiles of the skewness and the flatness factors defined by $S_u(x, y) = <u(x, y)^3 > /(< u(x, y)^2 >)^{3/2}$ and $F_u(x, y) = <u(x, y)^4 > /(< u(x, y)^2 >)^2$ at 20 nozzle widths downstream which is approximately the interaction zone. Both factors vary from the nearly Gaussian values ($S_{\rm u} \approx 0$, $F_{\rm u} \approx 3$) in the inner half of the boundary layer close to the jet centerline to

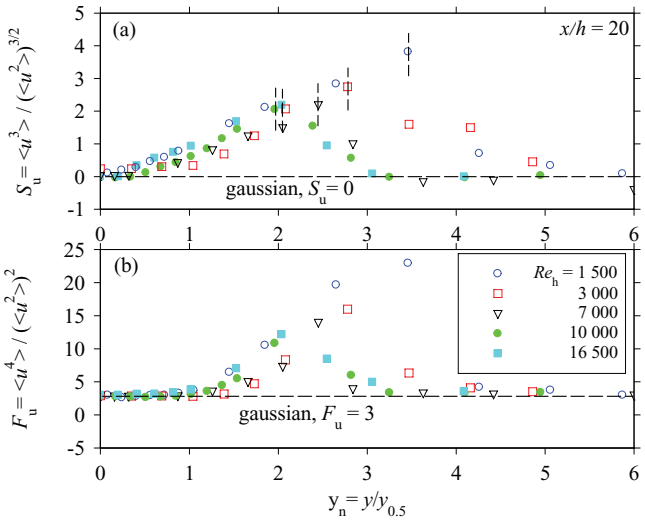

FIG. 14. Lateral profiles of (a) the skewness factors ($S_{\rm u}$) and (b) the flatness factors ($F_{\rm u}$) of the fluctuating velocity measured across the jet at $x/h = 20$. The dashed (- - -) line shows the maximum skewness in the outer boundary layer.

increasingly large values in the middle of the shear layers where they register local maximum values ($S_{u,max}$ and $F_{u,max}$) for all tested cases. That the near Gaussian values are found on the jet centerline shows that Re_h does not influence the turbulent statistics at $x/h = 20$. However, the influence of Re_h becomes apparent away from the axis, where the profiles of S_u and F_u are different for different cases. This becomes more conspicuous near the boundary-layer edges, which, in *ad hoc* terms is defined as the y-location where maximum skewness and flatness factors (e.g., Ref. 47) are detected by the probe.

Based on this rather crude definition, the low-*Re* jet exhibits significantly higher value of S_u and F_u than the high-*Re* counterparts. Notably, the case $Re_h = 1500$ produces larger peaks in the boundary layer, with $(S_{u,max}, F_{u,max}) \approx (4, 24)$ relative to (2, 12), respectively, for the case $Re_h = 16\,500$. Similarly, the $Re_h = 1500$ jet at the greatest width, at $(y_n \equiv y/y_{0.5}) \approx 3.5$, while the $Re_h = 16\,500$ jet measures only $y_n \approx 1.9$ which accords with greater spreading rate (Fig. 4) and higher shear layer growth rate (Fig. 6) for the former. Overall, both the skewness and the flatness factors indicate that the instantaneous velocity signals fluctuate with greater amplitude to characterize more intermittent flows for low-*Re* jets, as discussed further in Sec. IV D.

B. Isotropic turbulence statistics

In Sec. IV A, the impact of the downstream propagation of large-scale, energy bearing coherent eddies on the similarity behavior has been demonstrated. As these convect downstream, they cascade into smaller sized eddies until the jet is fully inviscid when the turbulent properties essentially behave in isotropic manner. In this situation, the net turbulent kinetic energy (E_k) acquired in the energy production zone is dissipated at the smallest (known as Kolmogorov) scale of turbulence (e.g., Ref. 27). To provide some insights into the behavior of these small-scale statistics of jets with various Re_h, the trends in isotropic turbulence statistics are presented in the following.

Figures 15 and 16 show the streamwise distributions of the Kolmogorov microscales $\eta(x)/h$ and Taylor microscales $\lambda(x)/h$. These data were acquired by a digital filtering scheme designed for resolving small-scale statistics in jet flows.[41] The data within the presented range of x/h show that the microscales obey similarity relationships of the form, $\eta(x) \sim x^{5/8}$ and $\lambda(x) \sim x^{3/4}$ in all measured jets, which is in accordance with Eqs. (25) and (26). The experimental data showing $\eta(x) \sim x^{5/8}$ demonstrates that the dissipative-scale eddies (η) are about an order of magnitude smaller than the inertial sub-range eddies (λ) for any given value of Re_h. This also accords with Kolmogorov-Oboukhov 1941 theory that the sub-range eddies (λ) are unaffected by the outer width scale ($y_{0.5}$)

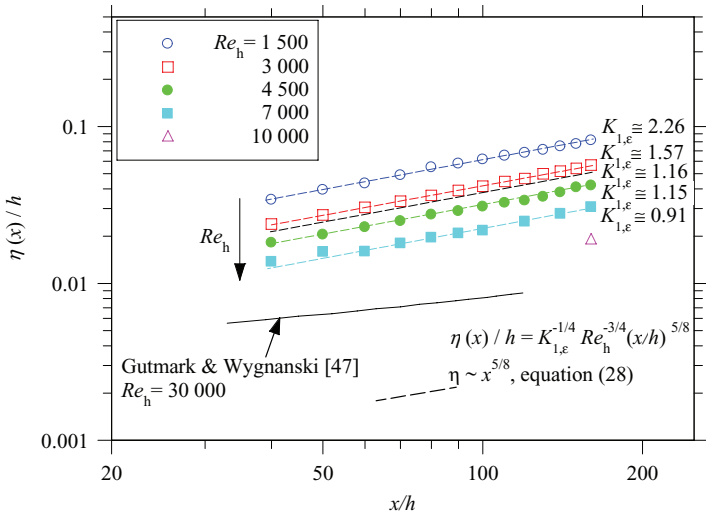

FIG. 15. Streamwise evolutions of the Kolmogorov microscales (η/h) as per Deo *et al.*[17]

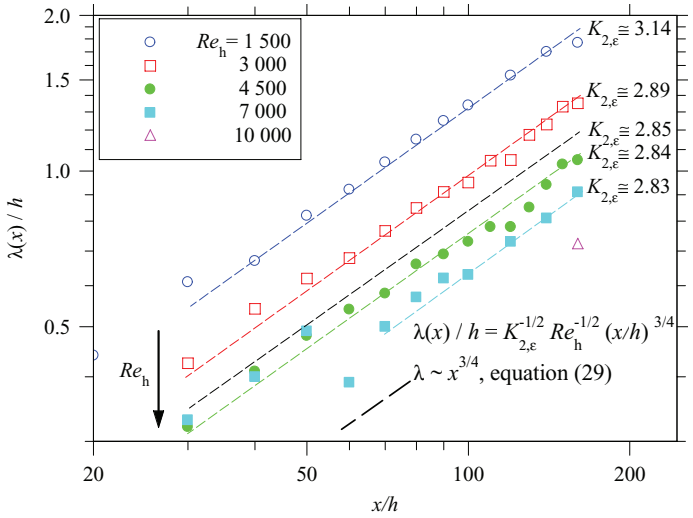

FIG. 16. Streamwise evolutions of the Taylor microscales (λ/h).

of the jet and generally large compared to the inner, viscous-dissipation sub-scale eddies (η), e.g., Ref. 27.

The present data also conforms to both microscales enlarging with increasing x/h for all cases, as expected. Thus the dissipative scales are all much smaller than those characterizing the energy of the turbulent fluctuations, and their relative size decreases with increasing Re_h. In spite of this, the Kolmogorov scales of all jets increase with increasing energy containing scales for fixed values of the Reynolds number. Perhaps of more interest, both microscales are found to be strictly Re_h-dependent as they scale uniquely with distinct values of their experimental constants, $K_{1,\varepsilon}$ and $K_{2,\varepsilon}$. Generally, these constants tend to decrease with increasing value of Re_h.

Figure 17 plots the streamwise evolutions of the Taylor microscale-based local Reynolds number $\mathrm{Re}_\lambda(x) = < u^2 >^{1/2} \lambda(x)/\upsilon$ for jets measured between $Re_h = 1500$ and 7000. Unlike the case of a circular jet where $Re_\lambda(x)$ is almost constant,[42] that for the present plane jet increases as $x^{1/4}$. The fourth-root scaling concurs with Mi *et al.*[42] for their plane jet data too, measured at $Re_h = 9125$, AR

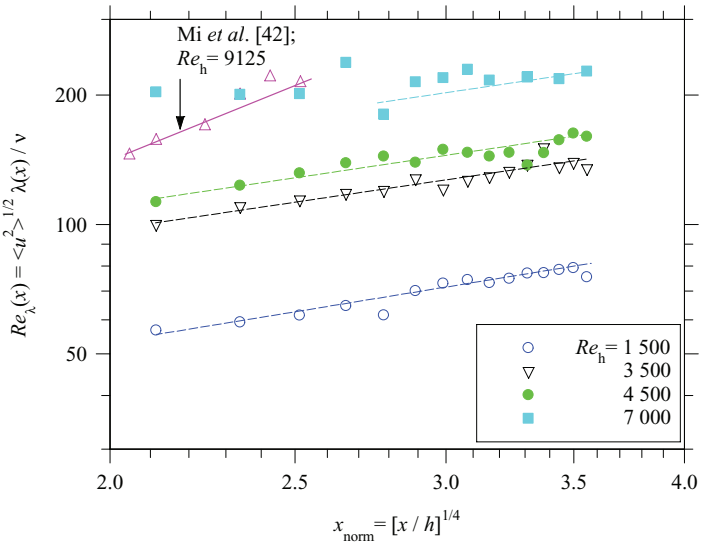

FIG. 17. Centerline variation of the local Taylor microscale-based Reynolds number, $\mathrm{Re}_\lambda(x) = < u^2 >^{1/2} \lambda(x)/\upsilon$. The plane jet data of Mi *et al.*[42] is included.

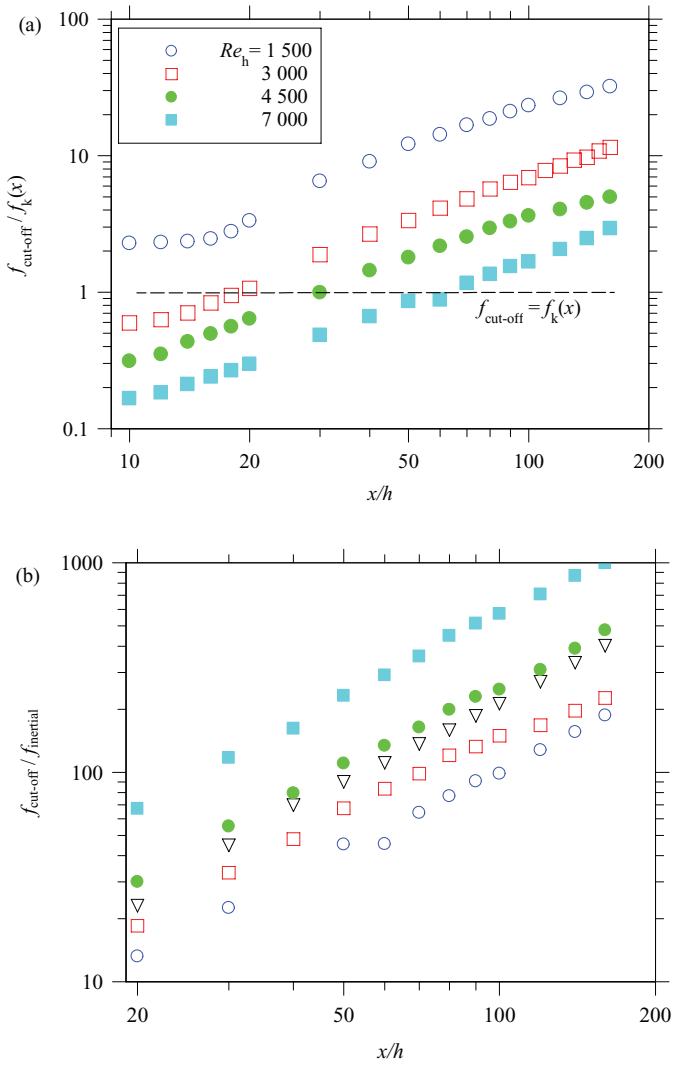

FIG. 18. The streamwise evolutions of the ratio of sampling frequency, $f_{cut\text{-}off}$ against (a) Kolmogorov frequency, $f_k = U_c(x)/[2\pi\ \eta(x)]$, (b) Eddy turnover Taylor frequency, $f_{inertial}$. Note: dashed line in (a) shows over-filtering for higher Re_h cases.

$= 36$, and $r/h = 1.80$. However, it is not surprising that the slope of the literature data contrasts that from the present investigation. No doubt this is attributable to the underlying differences in initial conditions of the jets of these investigations.[16,30,31] Apparently, the present data reveals significant disparities in the magnitude Re_λ that accord with different Re_h, with the general trend that the lower the Re_h, the smaller is the Taylor microscale-based local Reynolds number.

Figure 18(a) presents the streamwise evolution of the ratio of the sampling frequency $f_{cut\text{-}off}$ and Kolmogorov frequency $f_k(x) = U_c(x)/(2\pi\,\eta(x))$ for the cases $Re_h = 1500$–7000. It is self-evident that the present sampling frequency ($f_c = 9.2$ kHz) resulted in under-resolution of $f_k(x)$ in the near field of the higher Reynolds number cases, since $f_k > f_c$ for $x/h \leq 20$ for the cases $Re_h = 3000$, $x/h \leq 30$ for $Re_h = 4500$ and $x/h \leq 50$ for $Re_h = 7000$. A closer observation shows that similar effect was manifested in the data of Gutmark and Wygnanski[47] which too had a poor frequency response for adequate resolution of η. Hence their data has deviated from the $x^{5/8}$ line (see Fig. 15). However, for the present cases, f_K was fully resolved for $Re_h = 1500$ since $f_k < f_c$ everywhere within the present range of x/h. Figure 18(a) also embodies unambiguously the inversely varying relationship between f_k and x/h for the cases $Re_h \geq 3000$. Importantly, the eddy scale of jets measured at higher Re_h

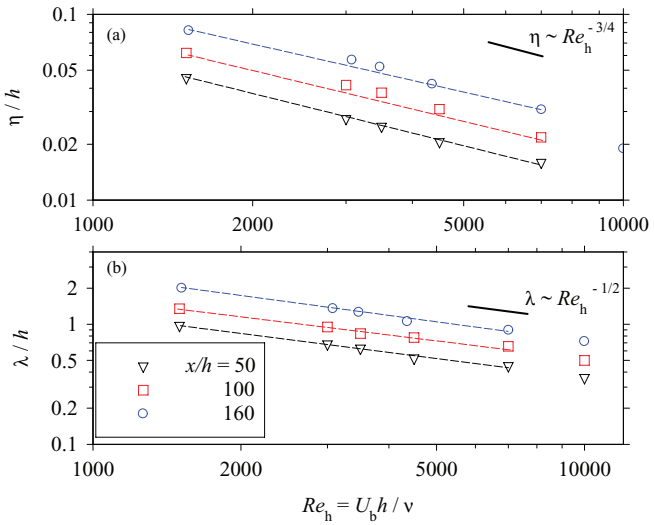

FIG. 19. The Re_h-dependence of (a) Kolmogorov scales (η), (b) Taylor microscales (λ) in the self-preserving field measured between $x/h = 50$ and 160.

exhibit greater frequencies of motion within the entire range of x/h, which perhaps indicates more rapid diffusion of the small-scale eddies for these more inviscid jets.

Figure 18(b) presents the streamwise evolutions of the ratio of the sampling frequency $f_{\text{cut-off}}$ and the mean eddy turnover frequency $f_{\text{inertial}} = (\varepsilon/\lambda^2)^{1/3}$ for $Re_h = 1500$–7000. Opposite to the trends noted for the frequency of Kolmogorov scales, the eddy motion denoted by Taylor microscales exhibit smaller turnover frequencies for the low-Re-jets compared to their high-Re counterparts. However, consistent with the frequency of Kolmogorov scales, the streamwise variation of f_{inertial} in locally isotropic flow also accords to the inversely proportional relationship where the eddy turnover frequency decreases with increasing x/h for all measured jets.

Figure 19 assesses the scaling of the Kolmogorov and Taylor microscales as a function of Re_h. Evidently, both scales exhibit inversely proportional relationships $\eta \sim Re_h^{-3/4}$ and $\lambda \sim Re_h^{-1/2}$, respectively (Figs. 19(a) and 19(b)). Clearly, as Re_h is decreased, the Taylor and Kolmogorov scales are indeed larger at identical downstream locations. This is perhaps associated with a greater fraction of the turbulent scales being moderated by the dominating viscous forces for low-Re jets, thus implying higher dissipation rates. These were reported previously for plane jets[10,17,30] and for round jets by Bogey and Bailey.[18]

Figures 20 and 21 presents the lateral distributions of η, λ, and ε measured in the self-preserving field at $x/h = 20$ for three Re_h-cases. For each jet, the microscales and turbulent kinetic energy dissipation rates are approximately invariant near the central axis of the jet, but then increase with lateral distance although the dissipation term declines rapidly toward the outer edge of the jet. Clearly, the actual magnitude of each micro-scale decreases with increasing Re_h, as expected. Reasonable agreement with measurements of Bradbury[45] is also met although the notable deviations from the present data are due to different measurement locations and initial conditions employed.[17,30] Furthermore, the present measurements over y-range $0 \le y_n \le 1.5$ appear to be over-filtered for the case $Re_h = 7000$, since f_k is larger than f_c in the inner boundary layer of this jet.

C. Explanation of flow structures by spectral analysis

The contrasting statistical properties depicted in the low and high Re-jets are further investigated using the power spectrum plots, $\Phi_{E_k}(k)$. The spectra are obtained by Fourier transformation of the one-dimensional streamwise turbulent kinetic energy, $E_k(x)$, where $\int_0^\infty \Phi_{E_k}(k)dk = \langle u \rangle^2$ and the wave number $k \equiv 2\pi f/U_c(x)$.

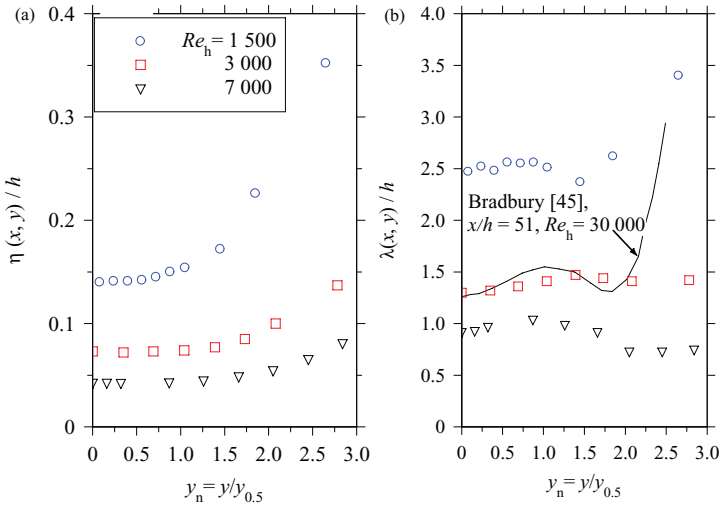

FIG. 20. The lateral distributions of (a) Kolmogorov scales (η), (b) Taylor microscales (λ) measured at $x/h = 20$.

Figure 22 presents the streamwise evolutions of $\Phi_{E_k}(k)$ for $Re_h = 1500$, 7000, and 16 500. In each spectral plot, the turbulent kinetic energy production zone is exemplified by the dominant peaks in $\Phi_{E_k}(k)$. These peaks extend over the region 0–10h for $Re_h = 1500$, 0–8h for $Re_h = 7000$, and 0–4h for $Re_h = 16\,500$. As is well-known, this near-field location corresponding to the potential core region is primarily responsible for generating the Kelvin–Helmholtz eddy structures that are primarily large-scale in nature. Propagating downstream, these eddies coalesce, grow in size and pair-up while they counter-rotate on the axis of the centerline, as detected previously in plane jet flows.[10,17] In present cases, the increasing axial range of the production zone with decreased Re_h signifies the dominance of more coherent, large-scale eddy structures in low Re-jets. This pattern also mirrors the enhanced peaks in turbulent kinetic energy profiles, which actually transformed away from the nozzle as Re_h was decreased [see Fig. 9 and Refs. 5–8). The near-field motion of large-scale eddy structures are deduced to elevate anisotropic disorders in low-Re jets, which are predominantly

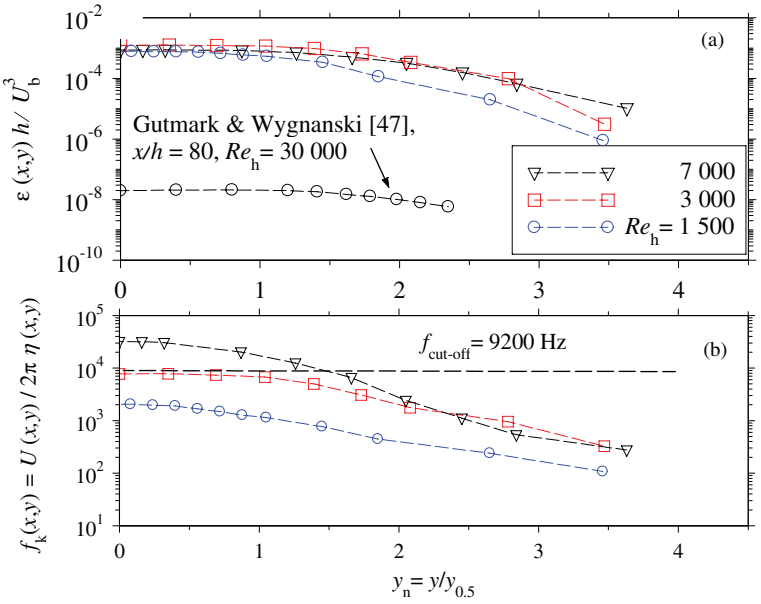

FIG. 21. The lateral distributions of (a) the dissipation of turbulent kinetic energy ($\varepsilon h/U^3{}_b$), (b) Kolmogorov frequency, $f_k(x, y) = U(x, y)/2\pi\eta$ at $x/h = 20$. The sampling frequency (f_c) is shown with the dashed line.

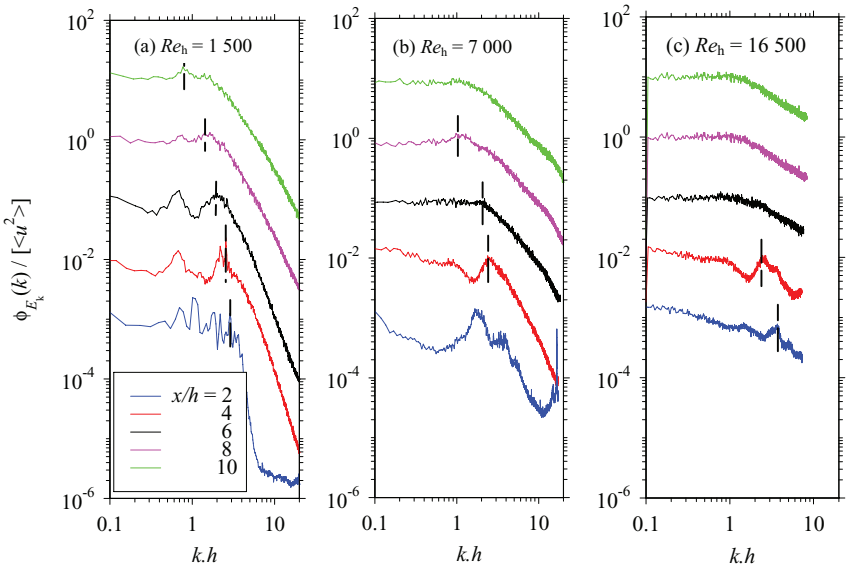

FIG. 22. Streamwise evolutions of turbulent kinetic energy spectra, $\Phi_{E_k}(k)$ on Re_h between $x/h = 0$ and 10. The dashed lines show energy production zones and nth spectra have been transformed in coordinate-axis by a factor of 10^n.

responsible for higher growth, larger entrainment, and greater mixing lengths as noted previously (Figs. 4–6).

To check the spectral behavior in the interaction and self-similar zones, Figure 23 displays the compensated power spectra $k^{5/3}\varepsilon^{-2/3}\Phi_{E_k}(k)$ versus kh for $Re_h = 1500$ and 16 500 over the downstream region, $x/h = 20$–100. The corresponding mean local Reynolds numbers at each downstream location is also shown. For a fully-developed, locally isotropic jet measured at sufficiently high Re_h, the small-scale eddy structures propagate with a length scale proportional to the inverse of their wave number and velocity scale, u_k proportional to $(\varepsilon/k)^{1/3}$. Based on this, dimensional analysis yields the Kolmogorov's law for the inertial sub-range $\Phi_{E_k}(k) \equiv u_k^2/k \sim \varepsilon^{2/3}k^{-5/3}$.[7,27,42] This clearly points out that the self-preservation of small-scale statistics is pertinent to the energy spectra satisfying the Kolmogorov's $k^{-5/3}$ exponential form. Evidently, in the present cases, the ordinate span of the spectra at any given x, where $\Phi_{E_k}(k) \sim k^{-5/3}$, is significantly larger for the high-Re_h jet. For example, at $x/h = 100$, the high-Re jet satisfies at over two decades of wave numbers exhibiting the $-5/3$ dependence, whereas only a decade of k-values are satisfied for the low-Re jet.

Indeed, the smaller span of the inertial sub-range in the spectra for the low-Re case is perhaps due to greater influence of viscosity on the small-scale eddy structures. This presumably prohibits the transition into fully-developed, homogeneous flows at axial distances $< 100h$, especially for $Re_h \leq 1500$ where the $-5/3$ region does not eventuate. From the same standpoint, the relative proportion of the turbulent energy per unit wave number contained in the small scale motions should be less for the low-Re jet, whereas those contained in the large scales should be greater. Since no net energy is produced in the far field, the larger equilibrium energy in the sub-range for high-Re must be compensated by smaller fraction of turbulent energy available for viscous dissipation, as found previously for plane jet flows, e.g., Refs. 10 and 17. This also concurs with the turbulent far-wake data of Zhou *et al.*,[43] where the energy dissipation was five fold greater for $Re = 9750$ relative to $Re = 2800$.

An ostensible implication of the present findings is that the sub-range of the spectra, the local Reynolds number at the designated location and the downstream location where the jet locks into the self-preserving state are closely related (Figs. 11 and 22). It is easily observable that our spectral plots mimic those of Uberoi and Freymuth[44] and Gourlay *et al.*[45] where similar effect of the local Reynolds number on the inertial sub-range of turbulent wake flow was reported. In our case, the sub-range with $k^{-5/3}$ dependence is completely absent for $Re_h = 1500$, until at least $x/h \approx 100$ when the local Reynolds number is sufficiently large (i.e., $Re_{y0.5}(x) \approx 4660$). By contrast, the jet with Re_h

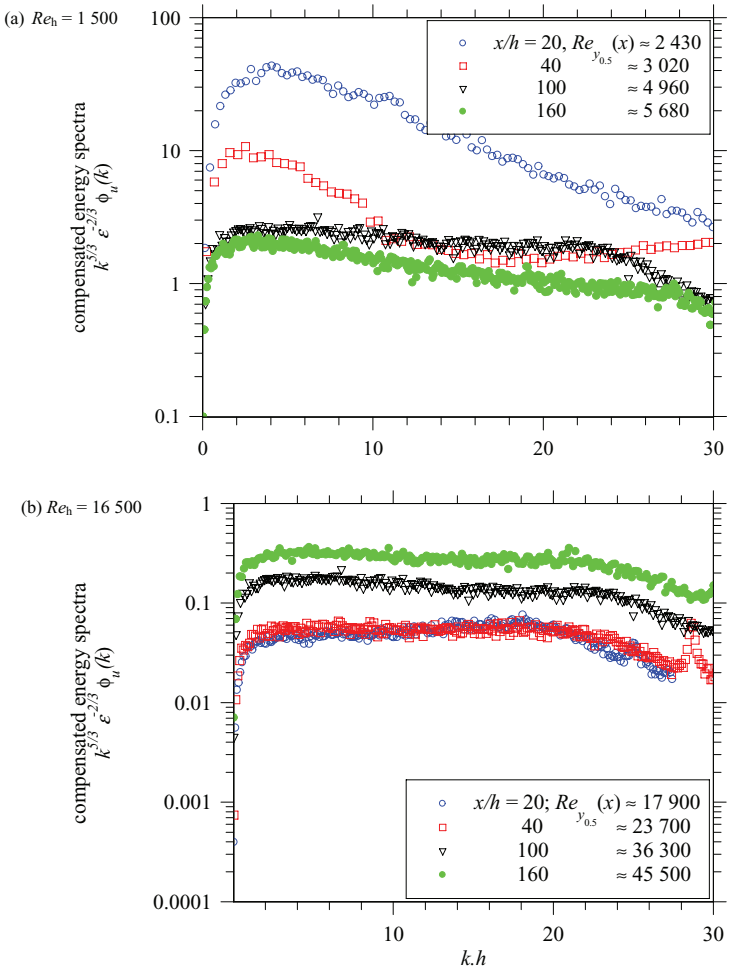

FIG. 23. Streamwise evolutions of compensated spectra of the turbulent kinetic energy, $k^{5/3}\varepsilon^{-2/3}\Phi_{E_k}(k)$ on Re_h and $Re_{y0.5}$ measured between $x/h = 20$ and 160. The width of the inertial sub-range where $\Phi_{E_k}(k) \sim k^{-5/3}$ for is characterized by the flat region on the ordinate axis.

$= 16\,500$ propagated only up to $x/h \approx 30$ to develop the $k^{-5/3}$ zone, which had actually acquired $Re_{y0.5}(x) \approx 18\,000$ (Fig. 8(a)), a value that appears to be well above the minimum threshold required to converge into the self-preserving state. This justifies why the turbulent kinetic energy became self-similar at $x/h = 100$ and 30 for jets measured at $Re_h = 1500$ and 16 500, respectively (see Fig. 9). It so appears that the plane jet evolves from the low to high Reynolds number similarity state only when $Re_{y0.5}(x)$ is sufficiently large to facilitate the $k^{-5/3}$ sub-range to emerge. Apparently, the present results also conform to George[23] theoretical deduction that the *high Reynolds number similarity applies only if there is an inertial sub-range in the spectrum so that the energy and scales of motion are effectively inviscid*. To our best knowledge, no prior experimental or numerical studies have demonstrated this phenomenon for a plane jet previously although it does explain the evolution of self-similar state closer to the nozzle for high-*Re* jets. Similar deduction was made by Johansson *et al.*[22] who reanalysed wake flow data to detect the disappearance of the sub-range when local Reynolds number declined below a minimum threshold value.

D. Further analysis of flow structure

Next we assess the flow structure of jets with different Re_h using the probability density functions (PDF) of the fluctuating velocity (u) on the jet centerline. Figure 24 displays the PDFs

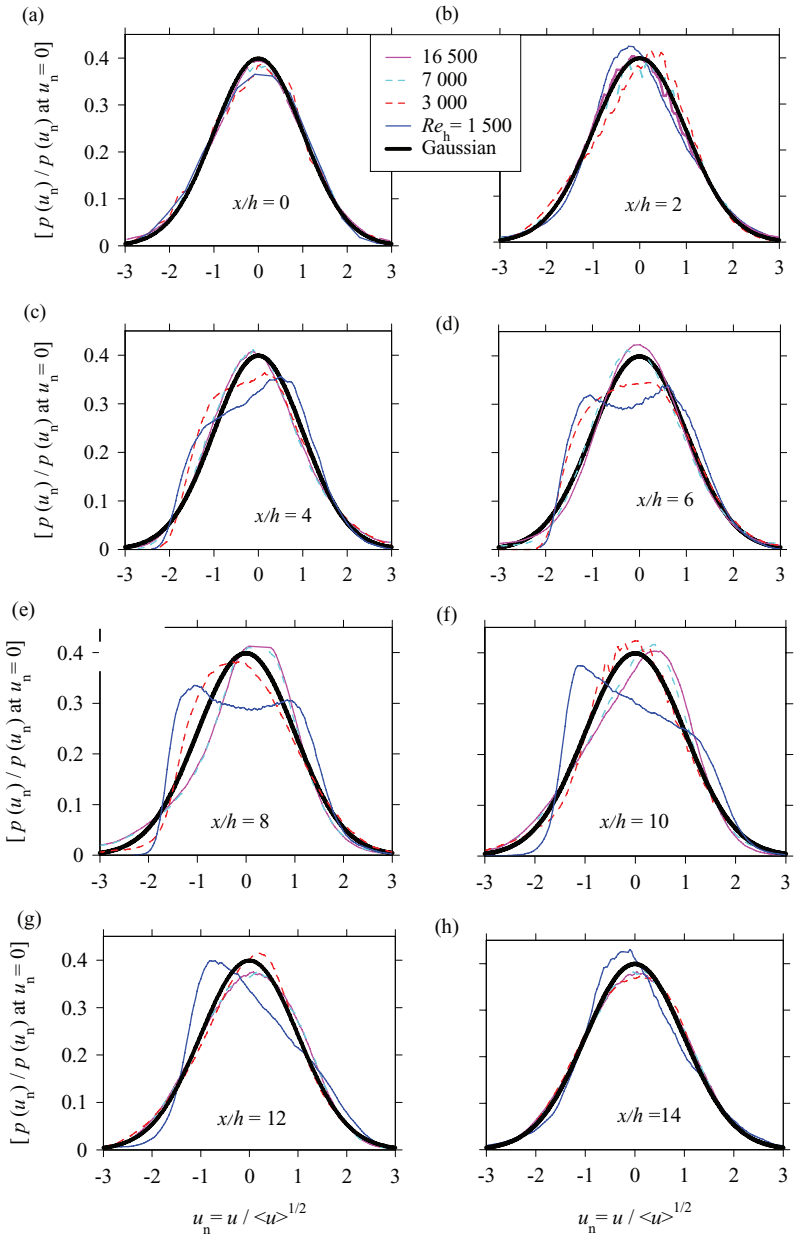

FIG. 24. The probability density functions PDF of centerline velocity fluctuations $u_c(x)$. The Gaussian distribution PDF $p(u_n) = 1/\sqrt{2\pi}\exp\left(-0.5\ln u_n^2\right)$ is shown.

in the near- (*a-f*) and interaction-fields (*g-h*). To compare the shapes, the x axis is normalised by $\langle u^2\rangle^{1/2}$ such that the integral $\int_{-\infty}^{+\infty} p(u_n)du_n = 1$, which are shown with the Gaussian form $p(u_n) = 1/\sqrt{2\pi}\exp\left(-0.5\ln u_n^2\right)$. Between the downstream locations 0 and $3h$, all PDFs resemble the Gaussian distribution. This is primarily due to the amplitude of the fluctuating velocity being relatively small within the potential core region of all measured jets. This also agrees qualitatively with our previous measurements that the skewness and kurtosis factors were found to be ≈ 0 and 3, respectively, see Ref. 17, that also confirmed low velocity fluctuations within the potential core region.

Between $x/h = 4$ and 12, the PDFs exhibit significant departures from Gaussian, which appear to be most pronounced for low-*Re* jets. The largest deviation found for $Re_h = 1500$ indicates the greatest skewness in the distribution of the instantaneous velocity signal as also confirmed by the larger peaks of turbulent kinetic energy spectra (cf., Fig. 9).

For the case $Re_h = 1500$, the PDFs in the near-field exhibit dual peaks which are especially pronounced between $x/h = 6$ and 8 although they disappear by $x/h = 10$. The bimodal behavior can be explained by revisiting our earlier study[17] that demonstrated the near field of the low-Re_h jet was composed of both symmetric and anti-symmetric modes of large-scale structures. In this jet both modes dominated the near-field flow in the initial flow region but the anti-symmetric mode disappeared for $x/h > 8$. Thus it is deduced that the bimodal behavior of the present PDFs between $x/h = 4$ and 8 is associated with the dual mode of large-scale structures present in the low-*Re* jet. This, however, contrasted the case of the high-Re_h jet where only the symmetric mode dominated the entire near-field that in the present investigation is shown by the single peaks of the PDF.

Interestingly enough we note that the jet measured at the lowest Re_h demonstrates consistently negatively skewed PDF between $x/h = 10$ and 12 which appears to vanish by $x/h = 14$. The negatively skewed instantaneous signal between 10 and 12 nozzle widths downstream depicts greater incursion of the low-velocity ambient fluid that is drawn rapidly into the low-*Re* jet by Biot–Savart law. This also accords the increased spurt in the turbulent kinetic energy noted previously (Fig. 9).

Figure 25(a) plots the intermittency factors, $\gamma \equiv < u^4 > /(< u^2 >)^2_{CL} / < u^4 > (< u^2 >)^2$ as a function of normalised distance ($y_n = y/y_{0.5}$) at $x/h = 20$. γ, which in our case is the ratio of the flatness factors along a given lateral distance (y) relative to its centerline (CL) value, has been deduced indirectly following the work of Wygnanski and Fielder.[46] The data show that the magnitude of intermittency decreases outside the outer edge of the jet, in agreement with the direct measurements of Gutmark and Wygnanski.[47] Importantly, the magnitude of γ also depends on Re_h. It is deduced that a generally higher γ value for any given y_n especially for the low Re_h-jet typifies a greater fraction of the jet that retains a turbulent state. This accords with Figure 10, where of the lateral distribution of turbulence intensity is not self-preserving for $Re_h = 1500$, at least within the measured range of x/h, and is perhaps attributable to increased instabilities within the shear-layer for this case.

The large-scale intermittency of the low-*Re* jet is also depicted in the auto-correlation function (R_{uu}) of the fluctuating velocity (Fig. 25(b)). The rapid oscillations in the tail of R_{uu} about the x axis, especially for the low-*Re* jet indicates greater instabilities in its shear layer, which aptly disappear at $x/h \geq 20$.

Since the spectral and autocorrelation plots (Figs. 22 and 25) are Fourier transform pairs (e.g., Ref. 48), the distinct peaks in power spectrum and the corresponding periodicity of R_{uu} at $x/h = 5$ for the jet measured at $Re_h = 1500$ confirms the dominant role of the large-scale, coherent vortices in the near field. By contrast, the reduced height of the peaks in spectra and the absence of periodicity at larger Re_h concur with less coherent vortical structures. Taken together, the present results supports a greater incursion of low-velocity ambient fluid for low-*Re* cases, where more coherent large-scale eddies for the (initially) low *Re*-jet are prevalent. This is consistent with the larger peaks in the turbulent kinetic energy distribution of jets measured at low Re_h (Fig. 9).

Figure 26 compares the PDFs of the velocity fluctuation on the jet centerline with those close to the edge of the jet measured at $x/h = 20$. Note that the edge is approximately the y-location of where maximum skewness and flatness factors are found. All measured PDFs close to the edge are characterized by significant deviations from the Gaussian, and are skewed to the left with the elongated tails on right side of the distribution. There is some evidence that as Re_h is increased, the PDFs become narrower and somewhat less skewed. By contrast, all PDFs on the jet centre closely align with the Gaussian, despite subtle differences between them due to experimental uncertainties.

V. FURTHER DISCUSSION

The present results have demonstrated that both the large and small-scale turbulence structure of plane jets scale with Re_h and the corresponding local Reynolds number. Statistical parameters such as the turbulent kinetic energy spectra, probability distribution functions, and autocorrelations signify

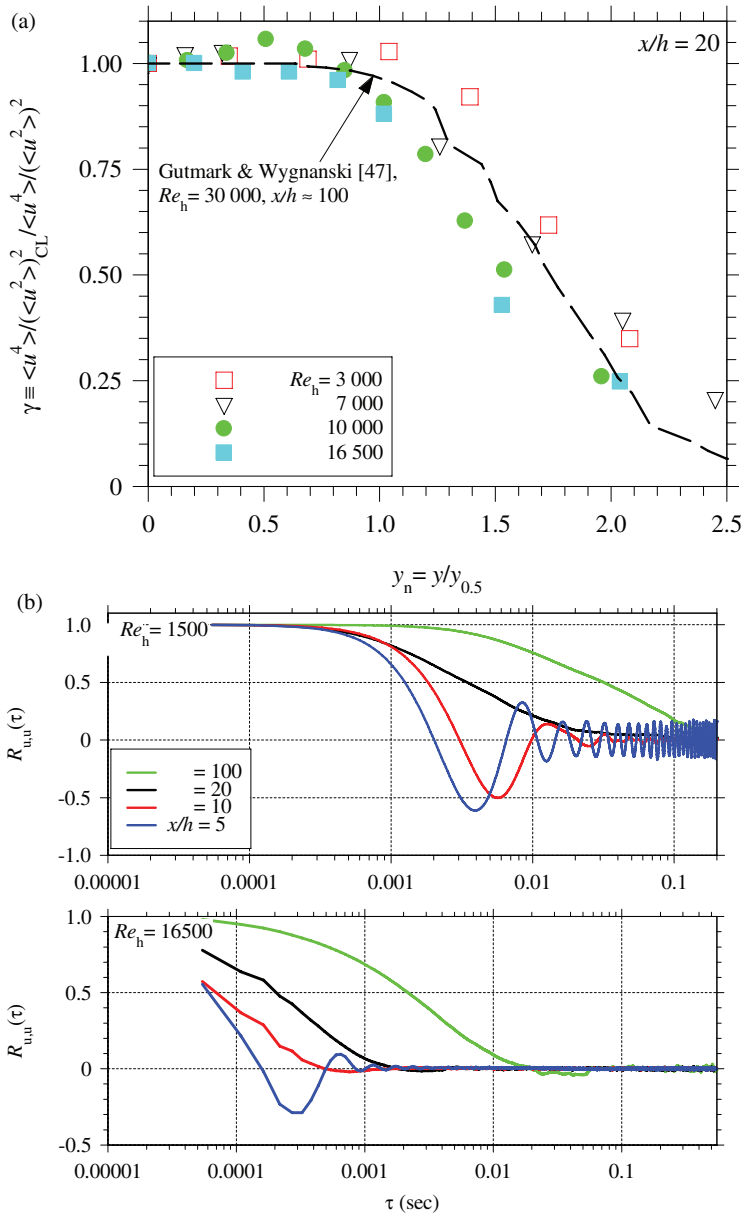

FIG. 25. (a) Lateral distribution of the intermittency factor, γ estimated indirectly from the flatness factor of the fluctuating velocity at $x/h = 20$ compared with Gutmark and Wygnanski's[47] direct measurements. (b) Autocorrelation functions, R_{uu} on the jet centerline for $Re_h = 1500$ and 16 500.

the differences in underlying flow structures of jets with varying Re_h. Support of this may also be drawn from the flow visualizations of Namar[49] and Dimotakis *et al.*,[50] which found similar changes in flow structures of rectangular and round jets measured at different Reynolds numbers. In their research, as Reynolds number was increased, the jet became narrower and produced increasingly disorganised and more three-dimensional eddy structures. These changes could be attributable to the corresponding increases in the overall enstrophy of the large-scale flow[29] as also demonstrated by the present results. Interestingly, the flow visualizations of Namar[49] found that the high *Re*-jet flow were composed of large-scale eddies superimposed on the small-scale eddies. Similarly, the present spectral plots indicated that increasing the Re_h causes a redistribution of the turbulent kinetic energy across a broader range of eddy structures, with comparatively smaller sizes. The change in

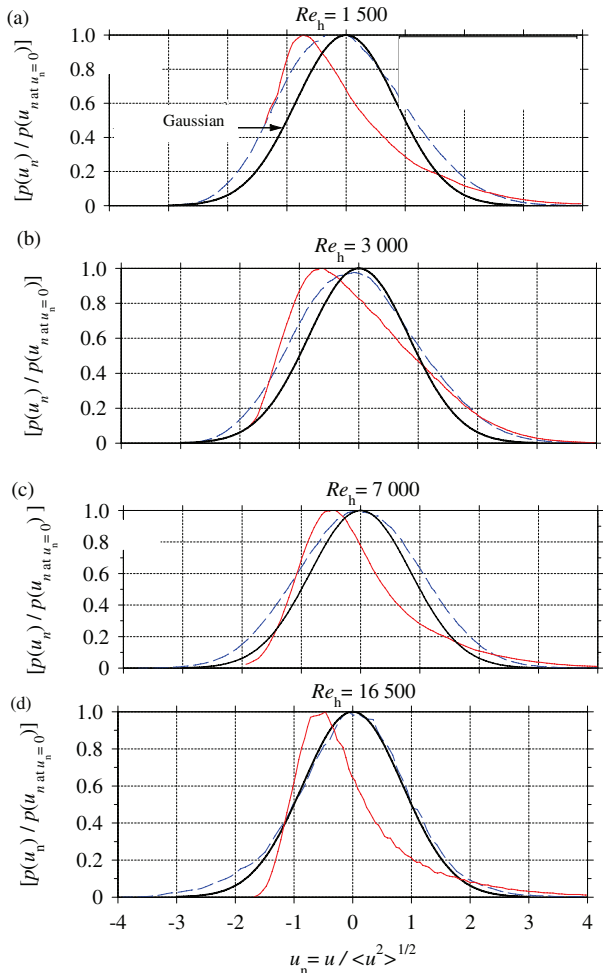

FIG. 26. Comparing the probability density function (PDF) of the fluctuating velocity (u) at $x/h = 20$ between the jet centerline (blue dash line) and edge (red full line). The y axis is normalised by $p(u_n)$ at $u_n = 0$ and Gaussian PDF is $p(u_n) = 1/\sqrt{2\pi}\exp\left(-0.5\ln u_n^2\right)$.

the relative role of the large and small scale eddies for different Re_h concurs with unique self-similar states of the present jets. Furthermore, the entrainment and shear-layer growth rates decreased with Re_h, thus suggesting that the role of smaller-scale eddies become less important (Figs. 5 and 6).

Based on previous literature,[18,53] the downstream development of large-scale eddy structures accedes with the boundary layer characteristics. As noted in the present work, the propagated jets with different Re_h possessed unique momentum thicknesses (Fig. 5), which also corresponded to unique growth rate of large-scale eddy structures (Fig. 7). It is deduced that a wider shear layer for the low Re_h jet promotes larger eddy sizes than those found for high-Re cases. This explains the higher entrainment and growth rate of shear layers, which in turn facilitates greater mixing lengths (Fig. 6). Indeed, the enhancement of spreading rates for low-Re jets are correlated with greater mixing rates that are initiated by the periodic production, advection, and interaction of large-scale eddies.[51]

In the present investigation, the low Re_h exhibited greater jet spreading rates, which led to the correspondingly large eddy viscosity (υ_T) (Fig. 27) and more coherent eddy structures as deduced previously. Thus a relatively smaller value of υ_T and the correspondingly larger turbulent Reynolds number ($Re_T = U_b h/\upsilon_T$) for low-Re jets further supports the reduced role of viscous forces governing the high-Re jets. Our analysis thus support the ansatz that, a high Reynolds number is a necessary criterion for self-preservation, so that the leading order viscous terms vanish at a critical downstream

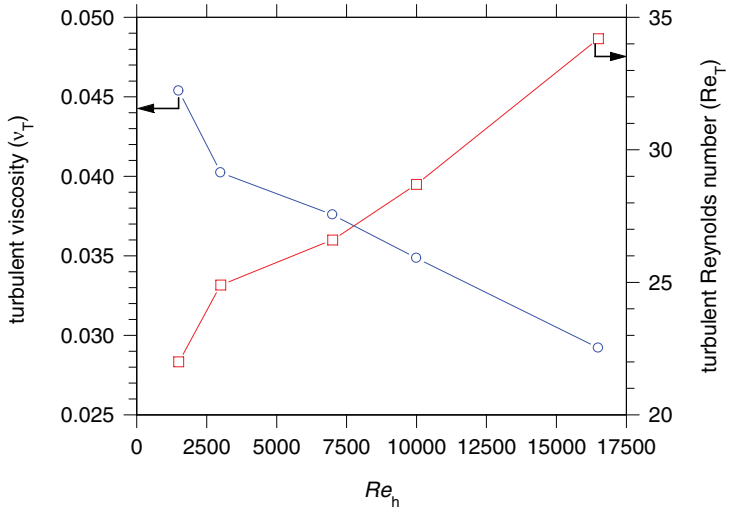

FIG. 27. The Re_h-dependence of turbulent viscosity (υ_T) and turbulent Reynolds number ($Re_T = U_b\, h\, /\upsilon_T$).

location beyond which any jet will lock itself into self-preservation.[23] Obviously, for the plane jet case, this is only possible when the local Reynolds number at that downstream location is sufficiently high due to the square root increase, and so indeed, the jet is nominally inviscid to allow the onset of self-preservation.

VI. CONCLUSIONS

This present study has investigated analytically and experimentally the effects of jet-exit and local Reynolds number on self-preservation of plane jets. The mass flow rates and momentum thicknesses are found to increase linearly with axial distance and the rate of this increase decreases asymptotically with Re_h, in accordance with the principles of preservation. The greater entrainment of the ambient fluid for low-*Re* jets coincides with higher magnitude and axial extent of the near-field peak in turbulent kinetic energy spectra, some-times termed the "production zone". For example this overshoot spanned a range of 10 x/h for the case $Re_h = 1500$, three times larger than the 4 x/h for the case $Re_h = 16\,500$. The integral length scale, which characterises the size of large-scale coherent eddies deduced from the autocorrelation functions, was found to increase linearly with x/h for all cases, as expected. However, the growth rate of large-scale eddies was found to decrease asymptotically with increasing Re_h. This is consistent with a decreasing dominance of larger eddies due to reduced role of viscosity for jets measured at high Re_h.

The mean local Reynolds number measured on the centerline and the turbulent local Reynolds number measured in the jet's shear layers are found to increase proportionally with $x^{1/2}$. This scaling applies to both the turbulent velocity field and spectra of turbulent kinetic energy in the self-preserving jet. Consequently, the significance of viscous terms in the momentum equations of high-*Re* jets become negligible closer to the nozzle than for low-*Re* counterparts. This concurs with the increasing importance of the local Reynolds number, which grows non-linearly with downstream distance for the case of a plane jet. Consequently, the streamwise evolution of the one-dimensional turbulent kinetic energy became self-similar at a shorter downstream distance for high Re_h cases.

The one-dimensional compensated turbulent kinetic energy spectra reveals the $-5/3$ Kolmogorov law in the spectra of jets at sufficiently great distance from the exit, but the span of this range increased with Re_h. This again highlighted the relevance of the local Reynolds number in achieving fully developed turbulence. Accordingly, the widener inertial sub-range for increased Re_h should correlate with reduced range of energy dissipation within the energy spectra, and thus lower dissipation rates reported previously by Suresh *et al.*[10] and Deo *et al.*[17] for plane jet flows. This also accords with similarity arguments that the dissipation (ε) of turbulent kinetic energy should obey the

form $\varepsilon \sim Re_h{}^3$ for self-preservation of a plane jet flow so that in high-*Re* jets, the cubical exponent means substantially greater dissipation and thus narrower range of wave numbers in dissipation region of the spectra. This happens as the acquisition of relatively large local Reynolds number, which subsequently dampens the role of viscosity, promotes the larger inertial sub-range and dissipation scales resolved for high-*Re* jets.

Based on present measurements, the relative growth of small-scale eddy structures (Kolmogorov and Taylor microscales) are found to increase linearly with downstream distance in the self-preserving field, albeit each being strictly dependent on Re_h. That is, an increase in Re_h reduces the size of small-scale eddy structures, as expected. Also importantly, the Taylor Reynolds number (Re_λ) increases with x as $Re_\lambda \sim x^{1/4}$ although jets measured at higher Re_h acquire larger values of Re_λ. Hence, discrepancies seen in the large and the small-scale statistics appear to be associated with the differences in gross initial conditions manifested by the source (or the jet-exit) Reynolds number Re_h, which governs the downstream evolution of the various forms of the local Reynolds number used to explain the transition to self-preservation of a plane jet. That is, the higher the Re_h, the faster is the growth of local mean, local turbulent or local Taylor Reynolds number. Thus, it is conjectured that the magnitude of Re_h is perhaps the most important parameter in predicting the transition to self-preservation, as also exemplified in autocorrelation and spectral plots that reflected discernable flow structures.

ACKNOWLEDGMENTS

R.C.D. acknowledges the Endeavour International Research Award, the Adelaide Achiever's Research Award, and ARC Linkage Grant for his Ph.D. studies. It is expressly stated that all experiments were undertaken at the School of Mechanical Engineering, The University of Adelaide, Australia. The analysis and completion of the final manuscript was undertaken by R.C.D. at the University of Southern Queensland (Springfield) that has been kindly supported by the Department of Mathematics and Computing. Finally, we thank both reviewers for their insightful comments which have strengthened the manuscript.

[1] H. Schlichting, "Laminare strahlausbreitung," ZAMM **13**, 260 (1933).
[2] F. Forthman, "Uber turbulente strahalusbreitung," In-genuer-Archiv **5**, 42–54 (1934) ["Turbulent jet expansion," National Advisory Committee for Aeronautics Technical Memorandum No. 789, National Aeronautics and Space Administration (1936)].
[3] W. Bickley, "The plane jet," Philos. Mag. **23**(7), 727–731 (1937).
[4] S. A. Stanley, S. Sarkar, and J. P. Mellado, "A study of the flow-field evolution and mixing in a planar turbulent jet using direct numerical simulation," J. Fluid Mech. **450**, 377–407 (2003).
[5] R. A. Antonia, W. B. Browne, S. Rajagopalan, and A. J. Chambers, "On organised motion of a turbulent planar jet," J. Fluid Mech. **134**, 49–66 (1983).
[6] F. C. Gouldin, R. W. Schefer, S. C. Johnson, and W. Kollmann, "Non-reacting turbulent mixing flows," Prog. Energy Combust. Sci. **12**, 257–303 (1986).
[7] S. B. Pope, *Turbulent Flows* (Cambridge University Press, United Kingdom, 2000).
[8] L. W. B. Browne, R. A. Antonia, S. Rajagopalan, and A. J. Chambers, "The interaction region of a turbulent plane jet," in *Proceedings of Structure of Complex Turbulent Shear Flows, IUTAM Symposium, Marseille*, 1982, pp. 411–419.
[9] G. P. Lemieux and P. H. Oosthuizen, "Experimental study of behavior of planar turbulent jets at low Reynolds numbers," AIAA J. **23**, 1845–1846 (1985).
[10] P. R. Suresh, K. Srinivasan, T. Sundararajan, and K. Das Sarit, "Reynolds number dependence of plane jet development in the transitional regime," Phys. Fluids **20**(4), 044105–044112 (2008).
[11] M. Klein, A. Sadiki, and J. Janicka, "Investigation of the influence of the Reynolds number on a plane jet using direct numerical simulation," Int. J. Heat Fluid Flow **24**, 785–794 (2003).
[12] I. Namar and M. V. Ötügen, "Velocity measurements in a planar turbulent air jet at moderate Reynolds numbers," Exp. Fluids **6**, 387 (1988).
[13] R. C. Deo, J. Mi, and G. J. Nathan, "Comparison of turbulent jets issuing from rectangular nozzles with and without sidewalls," Exp. Therm. Fluid Sci. **32**, 596 (2007).
[14] K. W. Everitt and A. G. Robbins, "The development and structure of turbulent plane jets," J. Fluid Mech. **88**, 563–583 (1978).
[15] J. Bashir and S. M. Uberoi, "Experiments on turbulent structure and heat transfer in a two-dimensional jet," Phys. Fluids **18**(4), 405–410 (1975).
[16] R. C. Deo, J. Mi, and G. J. Nathan, "The influence of nozzle aspect ratio on plane jets," Exp. Therm. Fluid Sci. **31**(8), 825–833 (2007).

[17] R. C. Deo, J. Mi, and G. J. Nathan, "The influence of Reynolds number on a plane jet," Phys. Fluids **20**(7), 075108 (2008).
[18] C. Bogey and C. Bailly, "Influence of nozzle-exit boundary-layer conditions on the flow and acoustic fields of initially laminar jets," J. Fluid Mech. **663**, 507–538 (2010).
[19] S. Russ and P. J. Strykowski, "Turbulent structure and entrainment in heated jets: The effect of initial conditions," Phys. Fluids A **5**(12), 3216–3225 (1993).
[20] R. A. Antonia and Q. Zhao, "Effects of initial conditions on a circular jet," Exp. Fluids **31**, 319–323 (2001).
[21] J. C. Mumford, "The structures of large eddies in fully developed shear flows. Part 1. The plane jet," J. Fluid Mech. **118**, 241–268 (1982).
[22] P. B. V. Johansson, W. K. George, and M. J. Gourlay, "Equilibrium similarity, effects of initial conditions and local Reynolds number on the axisymmetric wake," Physics of Fluids **15**(3), 603–617 (2003).
[23] W. K. George, "Some new ideas for similarity of turbulent shear flows," in *Proceedings of ICHMT Symposium on Turbulence, Heat and Mass Transfer, Lisbon, Portugal (1994)*, edited by K. Hanjalic and J. C. F. Pereira (Begell, New York, 1995).
[24] B. R. Ramaprian and M. S Chandrasekhara, "LDA measurements in plane turbulent jets," ASME J. Fluids Eng. **107**, 264–271 (1985).
[25] A. A. Townsend, *The Structure of Turbulent Shear Flow* (Cambridge University Press, 1956).
[26] R. A. Antonia, B. R. Satyaprakash, and A. K. M. F. Hussain, "Measurement of dissipation rate and some other characteristics of turbulent plane and circular jets," Phys. Fluids **23**(4), 695–700 (1980).
[27] N. Kolmogorov, "Local structure of turbulence in an incompressible viscous fluid at very high Reynolds numbers," Dokl. Akad. Nauk SSSR **30**, 299 (1941).
[28] G. Heskestad, "Hot-wire measurements in a plane turbulent jet," Trans. ASME, J. Appl. Mech. **32**, 721–734 (1965).
[29] L. J. S. Bradbury, "The structure of self-preserving turbulent planar jet," J. Fluid Mech. **23**, 31–64 (1965).
[30] R. C. Deo, "Experimental investigations of the influence of Reynolds number and boundary conditions on a plane air jet," Ph.D. dissertation, School of Mechanical Engineering, University of Adelaide, Australia, 2005, available at Australian Digital Thesis Program, see http://thesis.library.adelaide.edu.au/public/adt-UA20051025.054550/index.html.
[31] R. C. Deo, J. Mi, and G. J. Nathan, "The influence of nozzle-exit geometric profile on statistical properties of a turbulent plane jet," Exp. Therm. Fluid Sci. **32**, 545 (2007).
[32] F. H. Champagne, "The fine-scale structure of the turbulent velocity field," J. Fluid Mech. **86**(1), 67–108 (1978).
[33] P. Bradshaw, *An Introduction to Turbulence and its Measurements* (Pergamon, Oxford, United Kingdom, 1971).
[34] J. Tan-Atichat, W. K. George, and S. Woodward, *Handbook of Fluids and Fluids Engineering*, edited by J. A. Schetz and A. E. Fuhs (Wiley, New York, 1996), Vol. 3, Sec. 15.15, pp. 1098–1116.
[35] J. Hussein, S. P. Capp, and W. K. George, "Velocity measurements in a high-Reynolds-number, momentum-conserving, axisymmetric, turbulent jet," J. Fluid Mech. **258**, 31–75 (1994).
[36] K. B. M. Q. Zaman, "Far-field noise of a subsonic jet under controlled excitation," J. Fluid Mech. **152**, 83 (1985).
[37] C. J. Chen and W. Rodi, *Vertical Turbulent Buoyant Jets, A Review of Experimental Data* (Pergamon, Oxford, 1980), p.16.
[38] S. B. Pope, *Turbulent Flows* (Cambridge University Press, United Kingdom, 2002).
[39] H. Schlichting, *Boundary-Layer Theory* (McGraw-Hill, New York, USA, 1979).
[40] P. L. O'Neill, D. Nicolaides, D. Honnery, and J. Soria, "Autocorrelation functions and the determination of integral length with reference to experimental and numerical data," in *Proceedings of the Fifteenth Australasian Fluid Mechanics Conference (CD-ROM), The University of Sydney, Australia*, edited by M. Behnia, W. Lin, and G. D. McBain (Australasian Fluid Mechanics Society, Sydney, 2004).
[41] J. Mi, R. C. Deo, and G. J. Nathan, "Fast-convergent iterative scheme for filtering velocity signals and finding Kolmogorov scales," Phys. Rev. E **71**(6), 066304 (2005).
[42] J. Mi, M. Xu, and C Du, "Digital filter for hot-wire measurements of small-scale turbulence properties," Meas. Sci. Technol. **22**, 125401 (2011).
[43] Y. Zhou, R. A. Antonia, and W. K. Tsang, "The effect of the Reynolds number on the Reynolds stresses and vorticity in a turbulent far-wake," Exp. Therm. Fluid Sci. **18**, 291–298 (1998).
[44] M. S. Uberoi and P. Freymuth, "Turbulent energy balance and spectra of the axisymmetric wake," Phys. Fluids **13**, 2205 (1970).
[45] M. J. Gourlay, S. C. Arendt, D. C. Fritts, and J. Werne, "Numerical modelling of initially turbulent wakes with net momentum," Phys. Fluids **13**, 3783 (2001).
[46] I. Wygnanski and H. Fiedler, "Some measurements in the self-preserving jet," J. Fluid Mech. **38**, 577 (1969).
[47] E. Gutmark and I. Wygnanski, "The planar turbulent jet," J. Fluid Mech. **73**(3), 465–495 (1976).
[48] W. R. Quinn, "Upstream nozzle shaping effects on near field flow in round turbulent free jets," Eur. J. Mech. B/ Fluids **25**, 279–301 (2006).
[49] M. V. Namar, "An investigation of the structure of moderate reynolds number plane air jets," Ph.D. dissertation, Drexel University, 1986.
[50] P. E. Dimotakis, R. C. Miake-Lye, and D. A. Panpantoniou, "Structure and dynamics of round turbulent jets," Phys. Fluids **26**, 3185–3192 (1983).
[51] G. Krishnan and K. Mohseni, "An experimental and analytical investigation of rectangular synthetic jets," ASME J. Fluids Eng. **131**(12), 121101 (2009).
[52] T. Dracos, M. Giger, and G. H. Jirka, "Plane turbulent jets in a bounded fluid layer," J. Fluid Mech. **241**, 587–614 (1992).
[53] J. K. Eaton and J. P. Johnston, "A review of research on subsonic turbulent flow reattachment," AIAA J. **19**(9), 1093–1100 (1981).